

Dynamic in Static: Hybrid Visual Correspondence for Self-Supervised Video Object Segmentation

Gensheng Pei, Yazhou Yao, Jianbo Jiao, Wenguan Wang, Liqiang Nie, and Jinhui Tang

Abstract—Conventional video object segmentation (VOS) methods usually necessitate a substantial volume of pixel-level annotated video data for fully supervised learning. In this paper, we present HVC, a hybrid static-dynamic visual correspondence framework for self-supervised VOS. HVC extracts pseudo-dynamic signals from static images, enabling an efficient and scalable VOS model. Our approach utilizes a minimalist fully-convolutional architecture to capture static-dynamic visual correspondence in image-cropped views. To achieve this objective, we present a unified self-supervised approach to learn visual representations of static-dynamic feature similarity. Firstly, we establish static correspondence by utilizing a priori coordinate information between cropped views to guide the formation of consistent static feature representations. Subsequently, we devise a concise convolutional layer to capture the forward / backward pseudo-dynamic signals between two views, serving as cues for dynamic representations. Finally, we propose a hybrid visual correspondence loss to learn joint static and dynamic consistency representations. Our approach, without bells and whistles, necessitates only one training session using static image data, significantly reducing memory consumption ($\sim 16\text{GB}$) and training time ($\sim 2\text{h}$). Moreover, HVC achieves state-of-the-art performance in several self-supervised VOS benchmarks and additional video label propagation tasks. The source code and models are available at: <https://github.com/NUST-Machine-Intelligence-Laboratory/HVC>.

Index Terms—Self-Supervised, Video Object Segmentation, Visual Correspondence, Static-Dynamic Representation Learning

1 INTRODUCTION

VIDEO object segmentation (VOS) aims to separate and track objects of interest in videos, a task traditionally dependent on labor-intensive annotated data. The move towards self-supervised methods enables learning from unlabeled data, cutting the need for pixel-level annotations. Among these methods, visual correspondence learning has emerged as a particularly promising direction. Accordingly, self-supervised visual correspondence learning is introduced, which learns correspondence from raw videos without any external human supervision [1]–[14]. With the cooperation of correspondence learning across space and time, several downstream tasks, such as optical flow estimation [15]–[17], video object tracking [18]–[20], and VOS [21]–[24], have made considerable progress.

To design self-supervision signals, recent studies have employed various pretext tasks, including colorization [2], [9], cycle-consistency constraints [27]–[29], instance discrimination [30], [31], or image-level similarity [3]. Promising developments have been achieved by these approaches. Yet, a noise-based model [21] for pretext tasks could lead to local optima and overfitting [5]. To minimize noisy label effects, several studies [3], [31] have proposed dynamic correspondence learning, which is based on contrastive matching and draws inspiration from contrastive learning [32]. This approach involves contrasting the affinity of matched

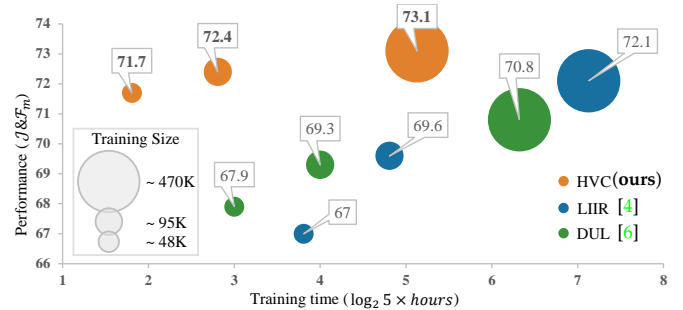


Fig. 1. **Self-supervised VOS performance comparison** on DAVIS₁₇ val-set. We adopt the same hardware device and training data [26] for a fair comparison. Bubble size indicates the size of training images. Taking less training time, our model outperforms state-of-the-art methods across all scales of data volume. HVC trained with 95K images achieves comparable performance to LIIR [4] delivered with 470K ones.

pixel pairs (*positive samples*) with that of unrelated pixel pairs (*negative samples*). Despite these efforts, there remains significant uncertainty in distinguishing between positive and negative samples. In response, recent works [1], [5], [6] have presented more accurate positive and negative sample mining techniques to address this challenge. Usually, spatio-temporal neighboring pixels are defined as positive pairs but still suffer from noise when the inter-frame feature differences are severe. To alleviate the aforementioned challenge, a set of solutions [33]–[36] directly utilize positive sample pairs for self-supervised feature representation learning, eliminating the need to grapple with the complexities of distinguishing between positive and negative samples. For various downstream tasks (e.g., classification [37], [38], detection [39], [40], and segmentation [41], [42]), the

- G. Pei, Y. Yao, and J. Tang are with Nanjing University of Science and Technology. (Email: {peigsh, yazhou.yao, jinhuitang}@njust.eud.cn)
- W. Wang is with Zhejiang University. (Email: wenguanwang.ai@gmail.com)
- J. Jiao is with University of Birmingham. (Email: j.jiao@bham.ac.uk)
- L. Nie is with Harbin Institute of Technology (Shenzhen). (Email: nieliqiang@gmail.com)

image-level global feature representations learned from this scheme still require dataset-specific fine-tuning and cannot be directly applied to dense video segmentation. Nevertheless, they undeniably pave the way towards self-supervised feature representation without using negative samples.

Existing self-supervised VOS approaches [1]–[7] focus on learning spatio-temporal feature representations from videos for dense segmentation tasks. However, one notable drawback of video-based correspondence learning is the relatively higher training costs compared to static images. Recently, some studies [35], [43], [44] have revisited MoCo [45] and proposed a multi-scale cropping strategy. This strategy enables models to learn static structure representations from images, making them applicable for VOS without the need for weight fine-tuning. However, it is worth noting that these methods [35], [43], [44] are built on the Vision Transformer (ViT) backbone approach [46], resulting in persistently high computational costs for training, and they do not effectively address the challenge of dynamic consistency.

In light of this context, one important question naturally arises: *Is it possible to learn spatio-temporal visual correspondence from static images only, thereby achieving self-supervised VOS in a more efficient manner?*

To address this question, we propose a method termed *hybrid visual correspondence* (HVC), which integrates *static* and *dynamic* visual correspondence learning from images into an elegant and efficient framework for self-supervised VOS. Departing from the conventional video data-driven methods, HVC eliminates the complexities of cross-frame reconstruction while attaining superior performance and resource efficiency. By exclusively leveraging static images, our approach exploits a vast reservoir of unlabeled images, showcasing diverse scenes, objects, and perspectives. These images act as an extensive repository of visual data, propelling the development of robust and widely applicable VOS models. However, a key challenge lies in the fact that unlike video data, which inherently encompasses dynamic information, static images lack the essential dynamic signals required for self-supervised VOS pretext tasks. It is not trivial to inject dynamic signals into static images.

Motivated by the aforementioned discussions, we propose a pseudo-dynamic learning strategy aimed at extracting pseudo-dynamic information from static images while incorporating their inherent static consistency present in these images. To achieve this, building upon a fully convolutional architecture, our model learns **i)** static consistency across image-cropped views and **ii)** dynamic consistency across pseudo-dynamic signals. Static consistency is attained by modeling similarities between image-cropped views, thereby bringing pixel pairs closer together in overlapping regions. We introduce pseudo-dynamic signals from static images to ensure dynamic consistency. This is accomplished through a meticulously designed pseudo-dynamic generation network, which determines the offset vector for each pixel in the cropped views of images with overlapping regions. To create positive masks, we leverage the determined coordinate relationships between cropped views of the images. These masks play a vital role in identifying the regions containing deterministic positive pixel pairs in both the image-cropped views (*static*) and the pseudo-dynamic signals (*dynamic*). This process enables the construction of

hybrid visual correspondence more effectively. Under a self-supervised paradigm, our approach ensures that the learned representations from only images achieve static-dynamic consistency, thereby fulfilling the stated aim.

We conduct extensive experiments and comprehensive ablation studies to validate the proposed approach. For self-supervised VOS, HVC demonstrates superior performance compared to state-of-the-arts, achieving \mathcal{J} & \mathcal{F}_m gains of **1.3%**, **1.0%**, **1.8%**, **2.0%**, and **6.7%** on the DAVIS₁₆ [24] val-set, DAVIS₁₇ [25] val-set, DAVIS₁₇ test-set, YouTube-VOS₁₈ [26] val-set, and YouTube-VOS₁₉ [47] val-set, respectively. HVC sets new state-of-the-art (**26.3%** \mathcal{J}_m) for the challenging VOST [48] benchmark. Furthermore, our approach yields competitive results in two additional tasks involving video label propagation, including part segmentation (**44.6%** mIoU on VIP [49]) and pose tracking (**61.7%** PCK@0.1 and **82.8%** PCK@0.2 on JHMDB [50]).

To sum up, the main contributions of this work include:

- 1) We propose a new self-supervised approach termed as hybrid visual correspondence (HVC), which effectively combines static and dynamic cues to tackle the challenge of label-free VOS. As shown in Fig. 1, HVC outperforms state-of-the-arts, achieving superior results while requiring notably less training data and time.
- 2) We introduce static and dynamic correspondence schemes that ensure the learned representations uphold static-dynamic consistency, a critical factor for VOS. Fig. 2 shows examples of mask propagation using HVC.
- 3) Our approach provides an elegant and efficient solution to liberate self-supervised VOS from its reliance on video data. By using only **static images** as training data, HVC surpasses the existing self-supervised strategies that depend on video data. Remarkably, HVC achieves exceptional performance utilizing a mere **16GB** GPU memory and a brief training duration of only **2 hours**.

2 RELATED WORK

2.1 Fully-Supervised Video Object Segmentation

VOS aims to segment universal foreground objects in video sequences, regardless of their semantic classes. In the inference stage, VOS is broadly classified into one-shot (or semi-supervised) VOS [51]–[54] and zero-shot (or unsupervised) VOS [55]–[59], depending on whether the object masks of the first frame target are provided. In the fully supervised VOS setting, inter-frame correspondence associations are established by learning feature representations to propagate semantic labels. Most existing approaches, whether based on matching [51], [60]–[62], propagation [63]–[66], or on-line fine-tuning [52], [67], [68], require large amounts of pixel-level annotated video datasets for supervised model training. These approaches typically use ImageNet [69] pre-trained backbones and fine-tune models on target datasets (e.g., YouTube-VOS [26] and DAVIS [24]) to achieve satisfactory performance. Unfortunately, this heavy reliance on expensive pixel-level annotated videos poses a significant limitation for fully supervised VOS methods.

Unlike the aforementioned approaches based on annotated videos, MaskTrack [64] stands out as one of the pioneering attempts to address VOS using only static images. It aims to achieve high-precision video segmentation by

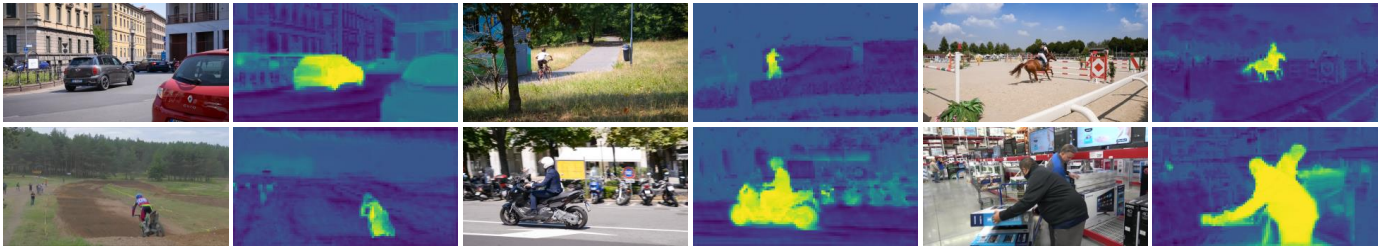


Fig. 2. **Learned representation visualization from HVC without any supervision.** Our proposed self-supervised hybrid visual correspondence learning highlights salient regions, suggesting the suitability of the HVC-learned representations for dense tasks such as video object segmentation.

leveraging static image data. However, it is worth noting that MaskTrack [64] is a fully supervised approach, which still requires many ground truth annotations for training. The quest for self-supervised methods that can learn VOS without relying on fully annotated videos has emerged as an active area of research. In this paper, we present a self-supervised VOS method that integrates both static and dynamic visual correspondence. Our approach addresses the challenge posed by limited labeled data in the VOS setting. By incorporating both static and dynamic information, HVC aims to enhance the accuracy and robustness of the segmentation process. This joint scheme overcomes the limitations posed by insufficient labeled data, offering a promising solution for self-supervised VOS.

2.2 Self-Supervised Video Object Segmentation

Self-supervised learning uses unlabeled data by constructing pretext tasks to learn visual representations. Typically, self-supervised visual representation learning does not focus on the final performance of the pretext tasks. Many works concentrate on discriminative methods [30], [32], [45], [70]–[72] towards instance-level classification. In this approach, each image is treated as a separate category, and the core idea is to bring feature embeddings of the same image view closer while pushing features of different images further apart. Recent works [33]–[35], [43] have demonstrated that self-supervised learning can acquire feature representations without instance discrimination. Notably, [43] attempts to address self-supervised VOS tasks by leveraging the powerful representation capabilities of ViT [46]. IKE [73] introduces a novel self-supervised learning framework that uses iterative knowledge exchange between deep learning and space-time spectral clustering, enhanced by longer motion chains, to achieve unsupervised object segmentation in videos. In recent years, the emergence of large-scale visual-language models like CLIP [74] has revealed their significant potential, leading to the development of language-guided self-supervised VOS methods [75], [76].

Recently, some studies [36], [44], [77] have revealed that constructing self-supervised pretext tasks using unlabeled image-level data [78], [79] can be extended to dense VOS scenarios as well. For instance, PixPro [36] leverages the consistency of pixel-level information across different augmented views of the same image. By training the model to predict pixel-level relationships and enforcing consistency constraints, the framework learns powerful visual representations. Building upon this idea, subsequent studies, SFC [77] and CrOC [44], have made substantial advancements in VOS by implementing a self-supervised training

strategy for static image cross-views, closely resembling the method introduced by PixPro [36]. These approaches have demonstrated noteworthy performance improvements in the VOS task. Although the cross-view visual representation can achieve static consistency, the lack of dynamic consistency is a common problem. We propose a hybrid visual correspondence approach that integrates both static and dynamic signals into the self-supervised learning process. Specifically, we inject dynamic signals into images to embed static and dynamic consistency within the original image-level visual correspondence learning. As a result, our method outperforms existing approaches trained on video datasets and achieves state-of-the-art performance across multiple VOS benchmark datasets.

2.3 Space-Time Correspondence Learning

Extracting inter-frame correlation has been a prominent and essential objective in computer vision, as it plays a vital role in various video applications, including optical flow estimation and object tracking. Recent methods [1]–[10], [12], [13] have made significant advancements in space-time video correspondence learning by leveraging self-supervised approaches. Color-consistency methods [2], [9], [21], drawing inspiration from video colorization, facilitate dynamic correspondence learning by comparing the affinity of current frame colors with the propagated future frame colors. Another line of approach utilizes circle-consistency constraint as their self-supervisory signals [1], [5], [6], [28], [29]. These methods aim to acquire static-dynamic feature representations by tracking both forward and backward pixels or regions among neighboring frames. Furthermore, certain methods [80]–[84] leverage optical flow [15], [16] to establish dynamic consistency constraints and learn features for dynamic correspondence. These approaches have significantly advanced self-supervised correspondence learning for video object segmentation. However, these solutions are exclusively designed for video sequences and heavily rely on inter-frame dynamic cues to guide self-supervised pretext tasks. In contrast, our hybrid visual correspondence learning approach does not require the acquisition of dynamic signals from video data. Instead, we subtly inject dynamic signals into the static images through a simple cropping operation. Significantly, the proposed approach outperforms the majority of video-based visual correspondence schemes.

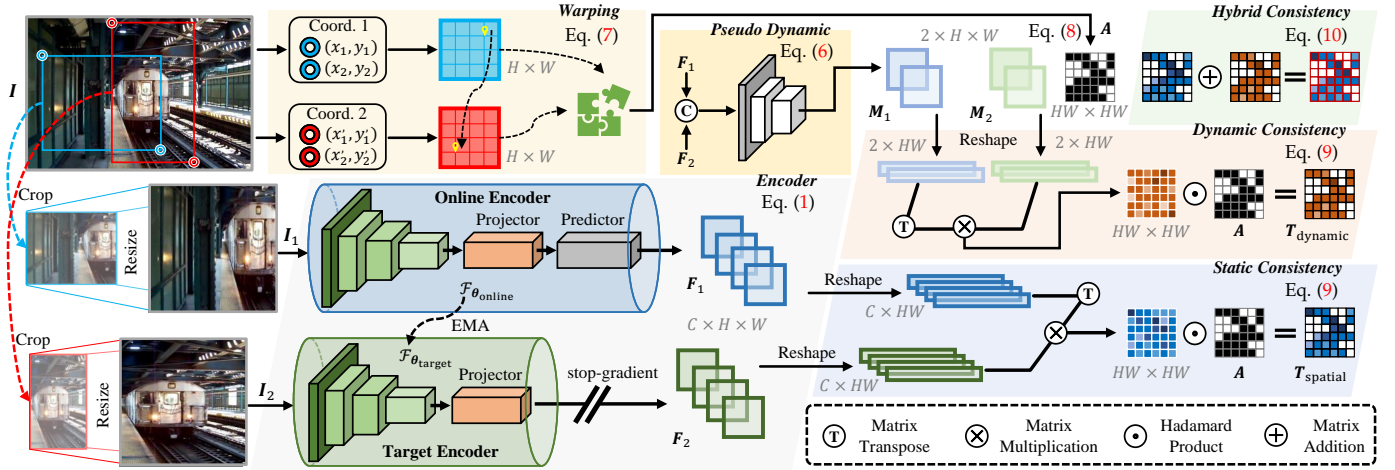


Fig. 3. **Architecture of the proposed HVC.** Given an image I , its pair of views I_1 and I_2 are obtained by crop-resize transformation. Two views are fed to the online and target networks, $\mathcal{F}_{\theta_{\text{online}}}$ and $\mathcal{F}_{\theta_{\text{target}}}$ (§3.1). The online network contains the additional projector and predictor heads to acquire feature maps F_1 and the target network appends only projector heads to receive feature maps F_2 . The pseudo-dynamic signal generation module receives F_1 and F_2 and outputs forward and backward pseudo-dynamic signals, M_1 and M_2 . Inter-feature and inter-dynamic similarities are combined with a positive sample mask to yield hybrid similarity (taking the negative, *i.e.*, final loss, see §3.2 for details).

3 THE PROPOSED METHOD

In this study, we introduce a hybrid visual correspondence framework designed to learn both static and dynamic correspondence solely from image data without any human annotations. In the following sections, we will introduce the overview of our framework (§3.1) illustrated in Fig. 3, then elaborate on the proposed method (§3.2). Additionally, we will delve into the implementation details (§3.3) of HVC.

3.1 Framework

In this study, we present an elegant and efficient visual correspondence learning method for video object segmentation, using label-free static images. Unlike conventional video correspondence learning methods that rely on video sequences, our approach aims to learn feature representations from static images and applies them to a self-supervised VOS task. Consequently, our model is trained only on static images. We show the architecture of the proposed method in Fig. 3 and provide the PyTorch-like style pseudo-code in Algorithm 1.

Given an image I , the pair of views $I_1, I_2 \in \mathbb{R}^{3 \times h \times w}$ is obtained by randomly cropping transformation [45]. HVC feeds image-cropped views into the online $\mathcal{F}_{\theta_{\text{online}}}$ and target $\mathcal{F}_{\theta_{\text{target}}}$ encoder networks. Both encoders comprise a backbone and a projector head. In particular, the online encoder brings in an additional predictor head to create an asymmetric structure between the online and target encoder networks, following the generalized methodology [85]. The projector and predictor heads are constructed with a space projection module, which consists of three consecutive 1×1 Conv layers (in this work, we set the output channels to 256, see §4.2). Here, a BN layer and a ReLU layer are inserted between neighbouring Conv layers to generate feature maps with a specific spatial resolution (set to 32×32 in this work).

Following [43], [45], the online encoder is updated by gradient, and we apply the stop-gradient operator to the target encoder. The target encoder parameters θ_{target} are updated in each training iteration by an exponential moving

average (EMA) of the online encoder momentum parameters θ_{online} . Hence, the whole encoder architecture is:

$$\theta_{\text{target}} \leftarrow m\theta_{\text{target}} + (1 - m)\theta_{\text{online}}, m \in [0, 1], \quad (1)$$

where m is a momentum coefficient, and the setting of its momentum update strategy is detailed in §3.3.

To prevent a cumbersome training strategy, we only employ positive pairs to perform feature embeddings without negative pairs, which has been proven effective by recent works [33], [34], [43]. The feature maps of the two cropped views from one image are computed by $\mathcal{F}_{\theta_{\text{online}}}$ and $\mathcal{F}_{\theta_{\text{target}}}$ and normalized by l_2 normalization as:

$$F_1, F_2 = l_2(\mathcal{F}_{\theta_{\text{online}}}(I_1)), l_2(\mathcal{F}_{\theta_{\text{target}}}(I_2)) \in \mathbb{R}^{C \times H \times W}. \quad (2)$$

We apply a simple contrastive loss to learn the feature representations and construct the baseline model for visual correspondence learning, *i.e.*, minimizing the distance (measured by cosine similarity) between the projected features. The loss function is defined as:

$$\mathcal{L} = -\frac{\langle F_1, F_2 \rangle}{\|F_1\|_2 \|F_2\|_2}, \quad (3)$$

where $\langle \cdot, \cdot \rangle$ denotes inner product. The feature maps of F_1 and F_2 do not match directly since they come from two different views after cropping and resizing. Therefore, the main issue addressed in Eq. (3) is finding the optimal positive pairs between F_1 and F_2 . In §3.2.2, we will elaborate on this in detail and present a simple solution to achieve image-based correspondence learning for self-supervised VOS.

3.2 Hybrid Visual Correspondence Learning

In recent years, self-supervised VOS has witnessed significant advancements, driven by the incorporation of various leading technologies such as *photometric reconstruction* [2], [6], [8], [9], [21], [31], *cycle consistency tracking* [1], [4], [12], [29], [56], [86], and *contrastive matching* [3], [5], [6], [31]. These methods share three key similarities: 1) They employ video data for training. 2) Their primary objective centers around spatio-temporal correspondence. 3) The affinity matrix serves as an intermediate variable for reconstruction.

Algorithm 1 HVC PyTorch-like pseudocode.

```

# fo, ft: online and target encoder networks
# r: positive radius
# m: momentum coefficient
# pseudo: pseudo dynamic network
# load two crop views and coordinates
for v1, v2, c1, c2 in loader:
  # online output BxCxHxW
  o1, o2 = fo(v1), fo(v2)
  # target output BxCxHxW
  t1, t2 = ft(v1), ft(v2)
  # compute hybrid loss
  loss = hybrid_loss(o1, t2, c1, c2, r) + \
         hybrid_loss(o2, t1, c2, c1, r)
  # back-propagate
  loss.backward()
  # update online and target parameters
  update(fo)
  ft = m * ft + (1.0 - m) * fo
  # update momentum coefficient
  update(m)

def hybrid_loss(o, t, c1, c2, r):
  # compute forward / backward pseudo-dynamic signals
  f_pd, b_pd = pseudo(o, t), pseudo(t, o)
  # compute the positive mask
  D = dist(c1, c2)
  A = (D <= r).detach()
  # compute static and dynamic similarities
  static = (torch.bmm(o.T, t) * A).sum()
  dynamic = (torch.bmm(f_pd.T, b_pd) * A).sum()
  # compute hybrid loss
  loss = - (static + dynamic) / (A.sum() + 1e-6)
  return loss

```

3.2.1 Self-Supervised VOS in Videos

Given the reference and query frames I_{ref} , I_{query} , we formulaically represent the affinity matrix \mathbf{S} as follows:

$$\mathbf{S}_{ref}^{query} = \text{softmax}_{row}(\mathbf{I}_{ref} \mathbf{I}_{query}^\top) \in [0, 1]^{hw \times hw}, \quad (4)$$

where softmax_{row} represent row-wise softmax. In this manner, the three self-supervised strategies (*photometric reconstruction* \mathcal{L}_{pr} , *cycle consistency* \mathcal{L}_{cc} , and *contrastive matching* \mathcal{L}_{cm}) can be expressed as follows:

$$\begin{aligned}
 \mathcal{L}_{pr} &= \|\mathbf{I}_{query} - \mathbf{S}_{ref}^{query\top} \mathbf{I}_{ref}\|^2, \\
 \mathcal{L}_{cc} &= \|\mathbf{S}_{ref}^{query} \mathbf{S}_{query}^{ref} - \mathbb{1}\|^2, \\
 \mathcal{L}_{cm} &= -\log \frac{\exp(\mathbf{S}(p, p^+))}{\sum_{p^-} \exp(\mathbf{S}(p, p^-))},
 \end{aligned} \quad (5)$$

where $\mathbb{1}$ is an identity matrix with the appropriate size. (p, p^+) indicate positive (matched) pixel pairs, and (p, p^-) denote negative (unrelated) pixel pairs. It becomes apparent that the current approaches heavily depend on the affinity matrix \mathbf{S} . However, the acquisition of \mathbf{S} is prone to interference from data noise [5].

If accurate correspondence between pixels can be acquired, the above affinity matrix-based methods could be largely improved. While existing methods primarily focus on learning correspondence between video frames, we propose to approach this in a different way. Specifically, we randomly crop two overlapped views from the same image, simulating a pair of consecutive frames within a video sequence. In this case, the overlapped regions are considered as positive samples to learn a pseudo-dynamic correspondence. This new pseudo-dynamic correspondence learning approach will be elaborated on below.

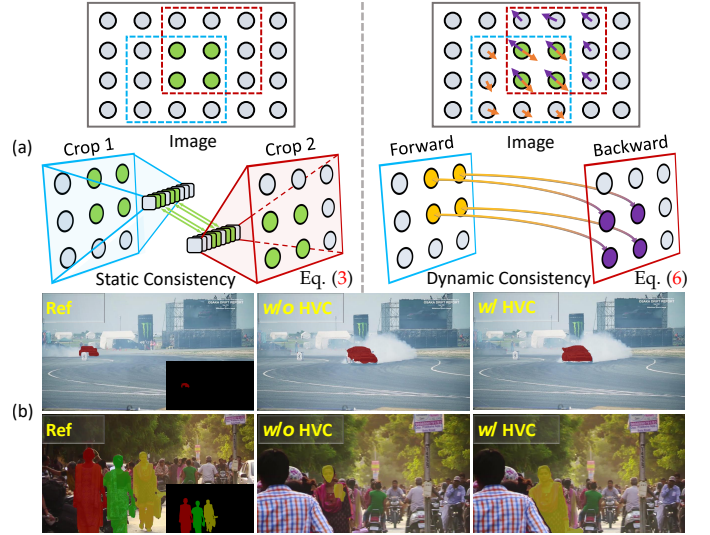


Fig. 4. (a) Illustration of **static and dynamic visual correspondence**. (b) Visualization of mask propagation.

3.2.2 Hybrid Visual Correspondence in Static Images

Indeed, static images inherently lack realistic dynamic information. However, it is feasible to generate pseudo-dynamic signals by altering the viewpoint through cropping mechanisms is feasible [16], [87]. In this section, we comprehensively describe the process of learning static-dynamic visual correspondence utilizing image data.

Pseudo-Dynamic Signal Generation. Existing video-based self-supervised VOS approaches have focused on learning the affinity matrix in video data due to its crucial role in ensuring static-dynamic consistency for VOS tasks. Our baseline approach constructed from Eq. (3) has a potential problem: the distance metric of the feature map only provides static consistency but not dynamic consistency.

To address the above issues, we introduce a hybrid visual correspondence approach, as depicted in Fig. 4(a). Specifically, given the projection features \mathbf{F}_1 and \mathbf{F}_2 , we construct Eq. (3) to provide static consistency constraint. To model dynamic consistency, we propose a pseudo-dynamic signal generation method, which involves fake video frames by cropping image patches followed by pseudo-dynamic signal estimation (similar to optical flow) between these cropped image views. Pseudo-dynamic signals are not direct optical flow estimations and guide the network in focusing on areas depicting motion between the pseudo-frames. The estimation module \mathcal{F}_{pseudo} consists of two consecutive convolutional layers with BN and ReLU. Particularly, our pseudo-dynamic signal generation method is seamlessly integrated into the entire framework without the need for any data annotation or conventional supervision. Together with Eq. (3), the loss function is defined as:

$$\mathcal{L}_{hybrid} = - \left(\underbrace{\frac{\langle \mathbf{F}_1, \mathbf{F}_2 \rangle}{\|\mathbf{F}_1\|_2 \|\mathbf{F}_2\|_2}}_{\text{static visual correspondence}} + \underbrace{\frac{\langle \mathbf{M}_1, \mathbf{M}_2 \rangle}{\|\mathbf{M}_1\|_2 \|\mathbf{M}_2\|_2}}_{\text{dynamic visual correspondence}} \right), \quad (6)$$

$$\mathbf{M}_1, \mathbf{M}_2 = \mathcal{F}_{pseudo}(\mathbf{F}_1, \mathbf{F}_2), \mathcal{F}_{pseudo}(\mathbf{F}_2, \mathbf{F}_1),$$

where $\mathbf{M}_1, \mathbf{M}_2 \in \mathbb{R}^{2 \times H \times W}$ indicate the forward and back-

ward pseudo-dynamic signals between F_1 and F_2 , respectively. Despite the absence of explicit optical flow computation, our HVC effectively leverages the spatial transformations between overlapping regions to simulate motion. The visual results are detailed in §4.3.4. Our objective is to maximize the similarity of static and dynamic features.

Positive Region Selection. Here, we will describe how we construct the positive pairs of feature maps (F and M). As described in Eq. (3), the sizes of two crop views in a given image differ, leading to shifts in feature positions after resizing. We randomly crop the image to obtain two views and record their original coordinates (top-left corner and bottom-right corner). These cropped views and their respective coordinates are the resized and transformed following a standard protocol [36]. Based on the spatial positions of the two cropped views in the original image, we generate the pixel coordinates of views after transformation as:

$$\begin{aligned} x_1^o, y_1^o &= \mathcal{W}(x_1, y_1), \\ x_2^o, y_2^o &= \mathcal{W}(x_2, y_2), \end{aligned} \quad (7)$$

where $\mathcal{W}(\cdot, \cdot)$ indicates warping operation, and $x^o, y^o \in \mathbb{R}^{H \times W}$ represent the transformed horizontal and vertical pixel coordinates, respectively.

Since the original coordinates of these views are known, we transform the projected features back to the original image space using the warping operation in Eq. (7). Subsequently, we can calculate the Euclidean distance \mathcal{D} between the two coordinate sets of feature maps in the original image space (see Fig. 3). This distance is used to gauge feature similarities, contributing to the model’s ability to establish visual correspondence. To define the spatial neighborhood of the local feature space, we set a positive radius r for the feature vectors that correspond to the identical cropped region (the overlapping region of the two crop views). Last, the positive region selection mask $\mathbf{A} \in \mathbb{R}^{HW \times HW}$ for the two crop views can be represented as:

$$\mathbf{A}(i, j) = \begin{cases} 1, & \text{if } \mathcal{D}(i, j) \leq r \\ 0, & \text{otherwise} \end{cases}, \quad (8)$$

where i, j represent the pixel coordinates from both crop views, and we set the positive radius r to 0.1 (see §4.2 for details). Unlike the affinity matrix-based approaches, we adopt a more direct optimization objective. To learn accurate visual correspondence from static images, we design the self-supervised signal (*i.e.*, \mathbf{A}), guided by the known coordinates of the two image-cropped views. Thus, in conjunction with Eq. (8), the static and dynamic visual correspondence methods described in Eq. (6) can be further expressed as:

$$\begin{aligned} \mathbf{T}_{\text{static}} &= \frac{\langle \mathbf{F}_1, \mathbf{F}_2 \rangle}{\|\mathbf{F}_1\|_2 \|\mathbf{F}_2\|_2} \odot \mathbf{A} \in \mathbb{R}^{HW \times HW}, \\ \mathbf{T}_{\text{dynamic}} &= \frac{\langle \mathbf{M}_1, \mathbf{M}_2 \rangle}{\|\mathbf{M}_1\|_2 \|\mathbf{M}_2\|_2} \odot \mathbf{A} \in \mathbb{R}^{HW \times HW}, \end{aligned} \quad (9)$$

where \odot denotes the Hadamard product. We ultimately aim to maximize the similarity matrices $\mathbf{T}_{\text{static}}$ and $\mathbf{T}_{\text{dynamic}}$.

Hybrid Loss for Visual Correspondence Learning. Learning visual correspondences from static images and applying them to dense video segmentation downstream tasks is not trivial. Dynamic signals between video frames are simulated by generating pseudo-dynamic signals using image-cropped views. This approach allows us to construct static

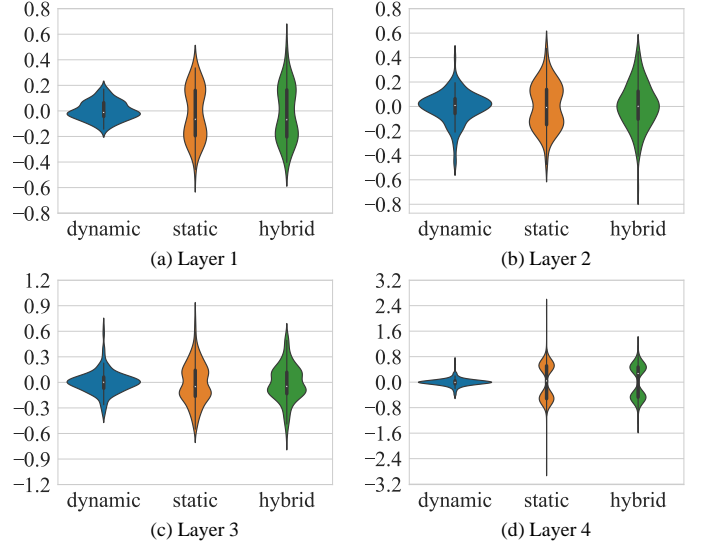


Fig. 5. Statistics of encoder weights (§3.2) at each layer of ResNet-18. The weights learned by **dynamic**, **static** and **hybrid** approaches are displayed from left to right in each violin plot.

and dynamic feature similarity in images, complementing our proposed model’s static and dynamic consistency. By combining Eq. (9), we rewrite Eq. (6) to fit into hybrid loss:

$$\begin{aligned} \mathcal{L}_{\text{static}} &= -\frac{\sum_{i=1}^{HW} \sum_{j=1}^{HW} \mathbf{T}_{\text{static}}(i, j)}{\sum_{i=1}^{HW} \sum_{j=1}^{HW} \mathbf{A}(i, j)}, \\ \mathcal{L}_{\text{dynamic}} &= -\frac{\sum_{i=1}^{HW} \sum_{j=1}^{HW} \mathbf{T}_{\text{dynamic}}(i, j)}{\sum_{i=1}^{HW} \sum_{j=1}^{HW} \mathbf{A}(i, j)}, \\ \mathcal{L}_{\text{hybrid}} &= \mathcal{L}_{\text{static}} + \alpha \mathcal{L}_{\text{dynamic}}, \end{aligned} \quad (10)$$

where α represents the weight factor of the dynamic loss $\mathcal{L}_{\text{dynamic}}$ (set to 1 by default, please refer to §4.2 for details). Using $\mathcal{L}_{\text{hybrid}}$ as the loss function, we establish the hybrid visual correspondence framework by employing Eq. (1). Examples of mask propagation are shown in Fig. 4(b).

To facilitate a more intuitive comparison of the dissimilarities in the learned feature representations of these approaches (*i.e.*, static, dynamic, and hybrid), we extract and visualize the feature weights of each encoder ($\mathcal{L}_{\text{static}}$, $\mathcal{L}_{\text{dynamic}}$, and $\mathcal{L}_{\text{hybrid}}$). As depicted in Fig. 5, the weights of dynamic correspondence learning appear more compact than the static ones. This compactness leads to a reduction in discrepancies among features obtained through the $\mathcal{L}_{\text{dynamic}}$ projection. A narrow distribution, as observed for the dynamic correspondence weights, indicates a higher degree of agreement among the features after the $\mathcal{L}_{\text{dynamic}}$ projection. On the other hand, the wider distribution of the static weights before the integration of dynamic correspondence learning implies a broader range of values and, subsequently, a more diverse set of feature representations. Upon integrating the hybrid correspondence, informed by both $\mathcal{L}_{\text{static}}$ and $\mathcal{L}_{\text{dynamic}}$, we observe a more integrated weight distribution that leverages the strengths of both correspondence types. The resulting feature representations are not only discriminative but also adept at generalizing across variations in motion and appearance in video sequences.

TABLE 1

Quantitative results for video object segmentation (§4.1.1) on DAVIS₁₇ [25] val-set. (#the number of images, #videos duration in hours) and (#image-level annotations, #pixel-level annotations) denote the dataset sizes for the self-supervised and supervised settings, respectively. For evaluation metrics, \cdot_m and \cdot_r are the mean and recall ones. $\mathcal{J}\&\mathcal{F}_m$ indicates the average of \mathcal{J}_m and \mathcal{F}_m . HVC-YT indicates that our model is pre-trained on YouTube-VOS₁₈ [26] train-set, the same as in Tables 2, 3, 4, 5, 8, 9 and 10.

Method	Publication	Backbone	Supervised	Traning Dataset	Size	$\mathcal{J}\&\mathcal{F}_m \uparrow$	$\mathcal{J}_m \uparrow$	$\mathcal{J}_r \uparrow$	$\mathcal{F}_m \uparrow$	$\mathcal{F}_r \uparrow$
Colorization [21]	ECCV-2018	ResNet-18	✗	Kinetics	(-, 800 hours)	34.0	34.6	34.1	32.7	26.8
TimeCycle [27]	CVPR-2019	ResNet-50	✗	VLOG	(-, 344 hours)	48.7	46.4	50.0	50.0	48.0
CorrFlow* [9]	BMVC-2019	ResNet-18	✗	OxUvA	(-, 14 hours)	50.3	48.4	53.2	52.2	56.0
UVC [28]	NeurIPS-2019	ResNet-50	✗	C + Kinetics	(118K, 800 hours)	60.9	59.3	68.8	62.7	70.9
MuG [29]	CVPR-2020	ResNet-18	✗	OxUvA	(-, 14 hours)	54.3	52.6	57.4	56.1	58.1
MAST [2]	CVPR-2020	ResNet-18	✗	YT	(-, 5.58 hours)	65.5	63.3	73.2	67.6	77.7
CRW [1]	NeurIPS-2020	ResNet-18	✗	Kinetics	(-, 800 hours)	67.6	64.8	76.1	70.2	82.1
ContrastCorr [8]	AAAI-2021	ResNet-18	✗	C + TN	(118K, 300 hours)	63.0	60.5	-	65.5	-
VFS [3]	ICCV-2021	ResNet-18	✗	Kinetics	(-, 800 hours)	66.7	64.0	-	69.4	-
JSTG [12]	ICCV-2021	ResNet-18	✗	Kinetics	(-, 800 hours)	68.7	65.8	77.7	71.6	84.3
CLTC* [31]	CVPR-2021	ResNet-18	✗	YT	(-, 5.58 hours)	70.3	67.9	78.2	72.6	83.7
DUL [6]	NeurIPS-2021	ResNet-18	✗	YT	(-, 5.58 hours)	69.3	67.1	81.2	71.6	84.9
SFC [77]	ECCV-2022	ResNet-18	✗	YT	(-, 5.58 hours)	71.2	68.3	-	74.0	-
SCC [5]	CVPR-2022	ResNet-18	✗	YT	(-, 5.58 hours)	70.5	67.4	78.8	73.6	84.6
LIIR* [†] [4]	CVPR-2022	ResNet-18	✗	YT	(-, 5.58 hours)	72.1	69.7	81.4	74.5	85.9
HVC-YT (ours)	-	ResNet-18	✗	YT	(-, 5.58 hours)	73.1	70.3	83.0	75.9	86.8
PixPro [36]	CVPR-2021	ResNet-50	✗	IN	(1.28M, -)	58.9	57.9	69.9	59.8	67.2
DINO [43]	ICCV-2021	ViT-B/8	✗	IN	(1.28M, -)	71.4	67.9	-	74.9	-
ODIN [88]	ECCV-2022	ResNet-50	✗	IN	(1.28M, -)	54.1	54.3	-	53.9	-
CLIP-S ⁴ [76]	CVPR-2023	ResNet-50	✗	IN	(1.28M, -)	54.6	52.3	-	56.8	-
CrOC [44]	CVPR-2023	ViT-S/16	✗	C	(118K, -)	58.4	56.5	-	60.2	-
HVC (ours)	-	ResNet-18	✗	C	(118K, -)	73.1	70.3	83.1	75.8	86.9
ResNet [89]	CVPR-2016	ResNet-18	✓	IN	(1.28M, -)	62.9	60.6	69.9	65.2	73.8
OSVOS [52]	CVPR-2017	VGG-16	✓	IN+D	(1.28M, 10K)	60.3	56.6	63.8	63.9	73.8
STM [51]	CVPR-2019	ResNet-50	✓	IN + D + YT	(1.28M, 164K)	81.8	79.2	88.7	84.3	91.8
XMem [53]	ECCV-2022	ResNet-50	✓	IN + D + YT	(1.28M, 164K)	86.2	82.9	-	89.5	-

*: 2x resolution. †: multi-step training. IN: ImageNet [69]. C: COCO [78]. D: DAVIS [25]. YT: YouTube-VOS [26]. TN: TrackingNet [90].



Fig. 6. **Qualitative results for video object segmentation (§4.1.1)** on DAVIS₁₇ [25] val-set (1st row), YouTube-VOS₁₈ [26] val-set (2nd row), DAVIS₁₆ [24] val-set (3rd row), and VOST [48] val-set (4th row). ‘%’ indicates progress status. Zoomed-in view for best.

3.3 Implementation Details

Architecture. Similar to previous studies [1]–[6], we use ResNet-18 [89] as the backbone to extract features. We remove the strides in the last two residual blocks (res_3 and res_4) like [27]–[29], [77]. The space projection module (see §3.1 for details) constructs the projector head and predictor head for feature embeddings on backbone output. We perform the l_2 normalization to obtain feature embeddings.

Training. We utilize COCO [78] as the static training dataset and train our hybrid visual correspondence model from scratch using a single NVIDIA A100 GPU. During training, the label-free raw images are randomly sampled. We create two randomly generated crops using only spatial augmentation, and resize all image crops to 256×256 , following [1]–

[6]. The entire model is implemented based on the PyTorch framework [91], with a mini-batch size of 128 for training over 20 epochs. The Adam optimizer [92] is adopted, with an initial learning rate of 10^{-3} and a weight decay of 0. At training time, the online encoder is optimized by gradients, while the target encoder updates its parameters by the moving average in each iteration. Following [45], the default value starts at 0.99 and increases gradually to 1.

Inference. Our HVC directly provides learned feature representations without any fine-tuning. Similar to [1], [6], [43], we adopt a versatile label propagation solution to evaluate VOS. Specifically, the first frame labels are provided for a video, and we compute the feature embedding similarity between the current frame and the previous frames (to

TABLE 2
Quantitative results for video object segmentation (§4.1.1) on YouTube-VOS₁₈ [26] val-set.

Method	Sup.	Mean	Seen		Unseen	
			$\mathcal{J}_m \uparrow$	$\mathcal{F}_m \uparrow$	$\mathcal{J}_m \uparrow$	$\mathcal{F}_m \uparrow$
Colorization [21]	✗	38.9	43.1	38.6	36.6	37.4
CorrFlow* [9]	✗	46.6	50.6	46.6	43.8	45.6
MAST [2]	✗	64.2	63.9	64.9	60.3	67.7
CLTC* [31]	✗	67.3	66.2	67.9	63.2	71.7
LIIR* [†] [4]	✗	69.3	67.9	69.7	65.7	73.8
CRW [1]	✗	69.9	68.7	70.2	65.4	75.2
DUL [6]	✗	69.9	69.6	71.3	65.0	73.5
HVC-YT (ours)	✗	71.6	70.0	72.1	67.3	77.0
HVC (ours)	✗	71.9	70.3	72.4	67.6	77.2
OSVOS [52]	✓	58.8	59.8	60.5	54.2	60.7
PreMVOS [93]	✓	66.9	71.4	75.9	56.5	63.7
STM [51]	✓	79.4	79.7	84.2	72.8	80.9

*: 2× resolution. †: multi-step training.

TABLE 3
Quantitative results for video object segmentation (§4.1.1) on DAVIS₁₆ [24] val-set.

Method	Sup.	$\mathcal{J} \& \mathcal{F}_m \uparrow$	$\mathcal{J}_m \uparrow$	$\mathcal{J}_r \uparrow$	$\mathcal{F}_m \uparrow$	$\mathcal{F}_r \uparrow$
Colorization [21]	✗	34.9	38.9	37.1	30.0	21.7
CorrFlow* [9]	✗	48.0	47.1	51.3	49.9	52.4
TimeCycle [27]	✗	53.5	55.8	64.9	51.1	51.6
MAST [2]	✗	68.8	69.3	82.7	68.3	78.9
MPFM [13]	✗	74.3	75.2	89.5	73.3	82.0
SPGO [‡] [80]	✗	78.8	80.2	-	77.5	-
HVC-YT (ours)	✗	80.1	79.1	91.6	81.0	88.6
HVC (ours)	✗	80.1	79.3	91.9	80.9	89.0
OSVOS [52]	✓	80.2	79.8	93.6	80.6	92.6
SiamMask [94]	✓	70.0	71.7	86.8	67.8	79.8
STM [51]	✓	89.3	88.7	-	89.9	-

*: 2× resolution. ‡: using additional optical flow.

provide first frame labels and previous predictions) to propagate labels to remaining video frames. Analogous to [77], we employ MoCo [45] as a baseline model to acquire rich semantic representations. To verify its effectiveness, HVC is evaluated on various challenging VOS datasets.

4 EXPERIMENTS

Following established conventions [1], [4]–[6], the evaluation model requires inferring the remaining frames’ pixel-level masks by providing the first frame mask of each video sequence. In §4.1, we utilize diverse video label propagation tasks to evaluate the learned representation of our model. The proposed critical components are extensively ablated in §4.2, and further analysis of HVC is conducted in §4.3. To maintain experimental impartiality, we supply a version of our model, denoted as HVC-YT, pre-trained on the YouTube-VOS₁₈ [26] training set. It should be noted that, unless specified, all primary results are derived from HVC trained exclusively on the static image dataset, *i.e.*, COCO.

4.1 Comparison with State-of-the-Art

In §4.1.1, we perform experimental comparisons of the proposed HVC with state-of-the-art VOS methods. Furthermore, we employ the proposed method to tackle two additional challenging video label propagation tasks: body part propagation in §4.1.2 and human pose tracking in §4.1.3.

TABLE 4
Quantitative results for video object segmentation (§4.1.1) on VOST [48] val-set. \mathcal{J}_m^{last} is the last 25% of the frames in a video.

Method	Sup.	$\mathcal{J}_m \uparrow$	$\mathcal{J}_r \uparrow$	$\mathcal{J}_m^{last} \uparrow$	$\mathcal{J}_r^{last} \uparrow$
MoCo [45]	✗	18.1	18.1	10.2	8.8
PixPro [36]	✗	16.8	16.8	10.0	9.5
DINO [43]	✗	18.8	18.9	10.4	9.4
CRW [1]	✗	22.3	23.0	13.3	12.6
DUL [6]	✗	23.9	23.9	14.6	13.7
SFC [77]	✗	20.6	21.0	11.8	11.1
HVC-YT (ours)	✗	26.0	26.9	14.5	13.0
HVC (ours)	✗	26.3	26.9	15.3	14.0
HODOR-Img [95]	✓	24.2	-	13.9	-
XMem [53]	✓	44.1	-	33.8	-
AOT [96]	✓	48.7	-	36.4	-

4.1.1 Results for Video Object Segmentation

Dataset. We evaluate performance on two publicly popular datasets: DAVIS₁₇ [25] and YouTube-VOS₁₈ [26], which contain 30 and 474 validation videos for performing the multi-object VOS task, respectively. We also conduct a comparison experiment for single-object VOS on DAVIS₁₆ [24]. In addition, we include the challenging VOST [48] benchmark, which comprises a validation set of 70 videos characterized by significant object transformation (breaking, occlusion, deformation, fast object motion, *etc.*) scenarios.

Metric. For quantitative comparison, we report the performance scores employing two official evaluation metrics [24], *i.e.*, region similarity \mathcal{J} and boundary accuracy \mathcal{F} . Given that YouTube-VOS consists of *seen* and *unseen* categories, we calculate the \mathcal{J} and \mathcal{F} scores separately for each category.

Evaluation on DAVIS₁₇. As shown in Table 1, we compare our proposed method with state-of-the-art self-supervised methods. Our HVC scores **73.1%** $\mathcal{J} \& \mathcal{F}_m$ and outperforms all other methods across all metrics. In contrast to LIIR [4], which utilizes a multi-step training strategy, HVC reaches **1%** $\mathcal{J} \& \mathcal{F}_m$ improvement with a more concise and efficient training approach (see Table 8). In addition, HVC delivers competitive performance compared to supervised methods.

Evaluation on YouTube-VOS₁₈. The results of HVC versus existing self-supervised methods on YouTube-VOS₁₈ [26] val-set are shown in Table 2. HVC achieves a new state-of-the-art and surpasses other self-supervised methods consistently. Compared to CRW [1] and DUL [6], our method achieves a **2.0%** higher mean score. Further, HVC is even superior to some well-known supervised methods [52], [93]. The high scores obtained for both *seen* and *unseen* categories highlight the robustness and adaptability of our approach.

Evaluation on DAVIS₁₆. As illustrated in Table 3, HVC outperforms all self-supervised methods in the single-object VOS setting. Compared to the state-of-the-art SPGO [80], which uses additional optical flow as auxiliary information, our approach improves by **1.3%** in terms of $\mathcal{J} \& \mathcal{F}_m$. HVC particularly achieves a comparable performance to the renowned supervised method OSVOS [52].

Evaluation on VOST. HVC achieves leading performance among self-supervised approaches, scoring **15.3%** \mathcal{J}_m^{last} , as detailed in Table 4. Compared to DUL [6], our approach improves by **2.4%/3.0%** in terms of $\mathcal{J}_m/\mathcal{J}_r$. HVC demonstrates superior capabilities when confronting the demanding VOST [48] benchmark (*e.g.*, occlusion and deformation).

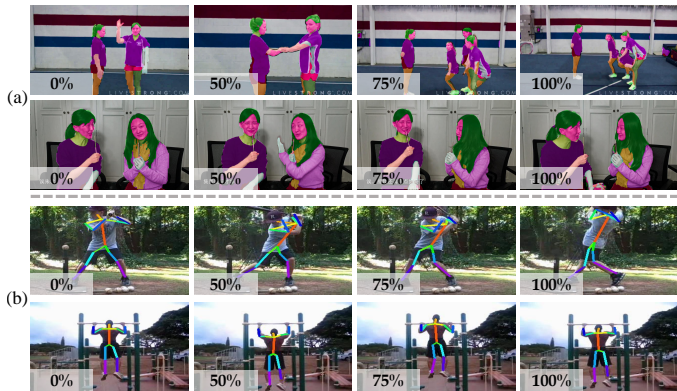


Fig. 7. Qualitative results of the proposed method for (a) body part propagation (§4.1.2) on VIP [49] val-set and (b) human pose tracking (§4.1.3) on JHMDB [50] val-set. Zoomed-in view for best.

TABLE 5
Quantitative results for part propagation (§4.1.2) on VIP [49] val-set and pose tracking (§4.1.3) on JHMDB [50] val-set.

Method	Sup.	VIP		JHMDB	
		mIoU ↑	PCK@0.1 ↑	PCK@0.2 ↑	
TimeCycle [27]	×	28.9	57.3	78.1	
UVC [28]	×	34.1	58.6	79.6	
CRW [1]	×	38.6	59.3	80.3	
VFS [3]	×	39.9	60.5	79.5	
CLTC* [31]	×	37.8	60.5	82.3	
PixPro [36]	×	29.6	57.8	80.8	
LIIR*† [4]	×	41.2	60.7	81.5	
SCC [5]	×	40.8	61.7	82.6	
HVC-YT (ours)	×	45.1	61.7	82.8	
HVC (ours)	×	44.6	61.7	82.8	
ResNet [89]	✓	31.9	53.8	74.6	
TSN [97]	✓	-	68.7	92.1	
ATEN [49]	✓	37.9	-	-	

*: 2× resolution. †: multi-step training.

Qualitative Results. Fig. 6 shows the video label propagation results from leveraging our learned visual correspondences. Our HVC has shown good segmentation results in confronting challenges such as occlusion, deformation, appearance changes, small objects, and fast motion.

4.1.2 Results for Body Part Propagation

Dataset. We evaluate HVC on the Video Instance Parsing (VIP) dataset [49] for body part propagation. The val-set split of the benchmark contains 50 videos focusing on propagating 19 body parts, e.g., arms and legs. Hence, this task demands a higher level of precision in matching compared to video object segmentation. We follow the same settings as CRW [1] and resize the video frames to 560×560 .

Metric. To evaluate the performance of our model on the semantic-level propagation task, we use the standard metric provided by [49], i.e., mean intersection-over-union (mIoU).

Evaluation on VIP. Table 5 (left) compares our model’s performance with existing self-supervised methods. Our HVC achieves superior performance compared to LIIR [4] and SCC [5] by 3.4% and 3.8% in terms of mIoU, respectively. Moreover, HVC significantly improves over the fully supervised model ATEN [49] by 6.7%, which is a dedicated method designed for the VIP [49] dataset.

TABLE 6
Quantitative results of proposed key modules (§4.2) on DAVIS_{16,17} [24], [25] val-set.

#	Static Visual Correspondence	Dynamic Visual Correspondence	DAVIS ₁₇	DAVIS ₁₆
			$\mathcal{J} \& \mathcal{F}_m \uparrow$	$\mathcal{J} \& \mathcal{F}_m \uparrow$
1			67.1	72.5
2	✓		70.6 (+3.5)	77.4 (+4.9)
3		✓	69.9 (+2.8)	77.0 (+4.5)
4	✓	✓	73.1 (+6.0)	80.1 (+7.6)

Qualitative Results. Fig. 7(a) presents samples depicting the visual results of body part propagation. Our model adeptly propagates each part mask onto analogous instances.

4.1.3 Results for Human Pose Tracking

Dataset. We conduct the human pose tracking task using the JHMDB [50] val-set, which contains 268 videos and entails detecting 15 human keypoints. Following the evaluation protocol of [1], [5], [28], we evaluate our model with video frames resized to a resolution of 320×320 .

Metric. We utilize the Possibility of Correct Keypoints (PCK) [97] as the quantitative evaluation metric, which measures the percentage of keypoints that are in close proximity to the ground-truth keypoints across different thresholds.

Evaluation on JHMDB. We show the quantitative results of HVC against others in Table 5 (right). HVC achieves consistent improvements over existing self-supervised methods on this challenging task that requires precise fine-grained matching. Remarkably, our model in PCK@0.1 and PCK@0.2 performs even better than the fully supervised baseline [89] (trained with labels) by 7.9% and 8.2%, respectively. Still, there is a gap between task-specific approaches (e.g., [97]).

Qualitative Results. The pose tracking visualizations in Fig. 7(b) affirms that HVC establishes the exact visual correspondence and effectively tracks human keypoints.

4.2 Ablation Studies

Elaborated ablation studies are conducted on DAVIS [24], [25] val-set to investigate our proposed approach.

Analysis of Critical Modules (Eq. (10)). To analyze the respective contributions of proposed core components (i.e., static and dynamic visual correspondence), we perform a thorough ablation study, shown in Table 6. Compared to the baseline (#1, MoCo [45]), adding the two visual correspondence modules proposed above improves the performance by 3.5% (#2) and 2.8% (#3) $\mathcal{J} \& \mathcal{F}_m$ on DAVIS₁₇, respectively. For the single object dataset DAVIS₁₆, two modules outperform the baseline by 4.9% (#2) and 4.5% (#3) in $\mathcal{J} \& \mathcal{F}_m$ score. The results in the ablation study show that learning static and dynamic visual correspondence (#4, HVC) facilitates semantic self-supervised feature representations.

Step between Images (§3.2). To investigate the impact of the amount of training data on HVC, we set four step sizes: 1, 5, 8, and 10. Step sizes 5, 8 and 10 mean that the COCO [78] dataset (118K) is sampled at corresponding image intervals, i.e., 5, 8 and 10 times less data volume. As shown in Table 7a, our method at step size 5 decreases only 0.9% and 0.6% $\mathcal{J} \& \mathcal{F}_m$ on DAVIS₁₆ and DAVIS₁₇, respectively, compared to step size 1. Remarkably, even with only 24K images for

TABLE 7

Ablation studies (§4.2) on DAVIS [24], [25] val-set. Best results are marked in gray, representing the default settings of HVC. For baseline selection, “Score A→Score B” refers to the score of the original semantic model and the score after joining our method.

#	Step Size	DAVIS ₁₇ $\mathcal{J}\&\mathcal{F}_m \uparrow$	DAVIS ₁₆ $\mathcal{J}\&\mathcal{F}_m \uparrow$	#	Augmentation Strategy	DAVIS ₁₇ $\mathcal{J}\&\mathcal{F}_m \uparrow$	DAVIS ₁₆ $\mathcal{J}\&\mathcal{F}_m \uparrow$	#	Weight Factor	DAVIS ₁₇ $\mathcal{J}\&\mathcal{F}_m \uparrow$	DAVIS ₁₆ $\mathcal{J}\&\mathcal{F}_m \uparrow$	#	Positive Radius	DAVIS ₁₇ $\mathcal{J}\&\mathcal{F}_m \uparrow$	DAVIS ₁₆ $\mathcal{J}\&\mathcal{F}_m \uparrow$
1	1	73.1	80.1	1	Random Crop	73.1	80.1	1	0.1	71.9	79.1	1	0.01	71.5	78.4
2	5	72.2	79.5	2	+Transformation	72.9	80.0	2	0.5	72.6	79.6	2	0.10	73.1	80.1
3	8	71.7	79.0	3	+Color Jittering	71.0	78.3	3	1.0	73.1	80.1	3	0.30	72.8	79.9
4	10	71.2	78.8	4	+Gaussian Blur	71.4	78.9	4	2.0	73.0	80.0	4	0.70	72.2	79.3

(a) Step between Images (b) Data Augmentation (c) Dynamic Loss (d) Positive Discriminant

#	Pre-training Dataset	Is Video	Dataset Size	Best r	DAVIS ₁₇ $\mathcal{J}\&\mathcal{F}_m \uparrow$	DAVIS ₁₆ $\mathcal{J}\&\mathcal{F}_m \uparrow$	#	Hidden Dimension	DAVIS ₁₇ $\mathcal{J}\&\mathcal{F}_m \uparrow$	DAVIS ₁₆ $\mathcal{J}\&\mathcal{F}_m \uparrow$	#	Semantic Model	DAVIS ₁₇ $\mathcal{J}\&\mathcal{F}_m \uparrow$	DAVIS ₁₆ $\mathcal{J}\&\mathcal{F}_m \uparrow$
1	YouTube-VOS [26]	✓	447K	0.10	73.1	80.1	1	128	72.5	79.7	1	MoCo [45]	67.1→73.1	72.5→80.1
2	MSRA10k [98]	✗	10K	0.10	71.1	78.4	2	256	73.1	80.1	2	PixPro [36]	59.2→70.0	62.8→77.7
3	PASCAL VOC [79]	✗	17K	0.10	72.0	78.7	3	512	72.9	80.0	3	SimSiam [34]	67.0→71.5	72.7→79.3
4	COCO [78]	✗	118K	0.10	73.1	80.1	4	1,024	72.1	78.9	4	DINO [43]	65.8→70.9	72.4→79.6

(e) Searching Dataset & Positive Radius (f) Space Projection (g) Baseline Selection

training, HVC still outperforms the top-performing LIIR [4] that uses the YouTube-VOS₁₈ dataset with all frames (470K).

Data Augmentation (§3.3). The ablation study, as presented in Table 7b, thoroughly investigates the effects of diverse data augmentation strategies on the efficacy of HVC. Singular random cropping is the most effective strategy, echoing findings from preceding relevant studies [3], [77]. Notably, adding color jittering or Gaussian blur significantly deteriorates model performance. Furthermore, additional transformations (*e.g.*, affine and perspective) have little influence on performance yet incur increased computational overhead.

Dynamic Loss (Eq. (10)). As shown in Table 7c, we conduct an ablation study, examining the influence of the dynamic loss weight factor on performance. We observe that HVC achieves optimal results when α equals 1.0. Conversely, if α is set below 1.0, there is a notable decrease in performance. The empirical evidence suggests that assigning equivalent significance to both static and dynamic losses fosters a harmonized feature representation within our model.

Positive Discriminant (Eq. (8)). In Table 7d, we investigate the impact of different positive radius on performance. The positive discriminants are determined by the coordinates of the two crop views, providing supervision for visual correspondence learning. Fig. 8 illustrates the feature distances between crop views from different datasets and includes the number of positive samples corresponding to each r -value. A larger positive radius leads to an increase in too many wrong positive pairs, resulting in performance degradation. Conversely, a smaller radius makes the model overly strict and thus reduces the number of positive examples, which leads to more performance reduction. When the positive radius is set to 0.1, HVC reaches the best results on both DAVIS₁₇ and DAVIS₁₆ (*i.e.*, 73.1% and 80.1% over $\mathcal{J}\&\mathcal{F}_m$).

Searching Dataset & Positive Radius (Eq. (8)). To investigate the effect of different datasets on HVC, we perform pre-training on two additional image-level datasets (*i.e.*, MSRA10k [98], PASCAL VOC [79]) and a widely-used video-level dataset, *i.e.*, YouTube-VOS [26] (treating frames as separate images). As shown in Table 7e, the performance of our method trained on COCO is comparable to the video-level dataset YouTube-VOS₁₈, despite COCO (118K) having only a quarter of the number of images as YouTube-

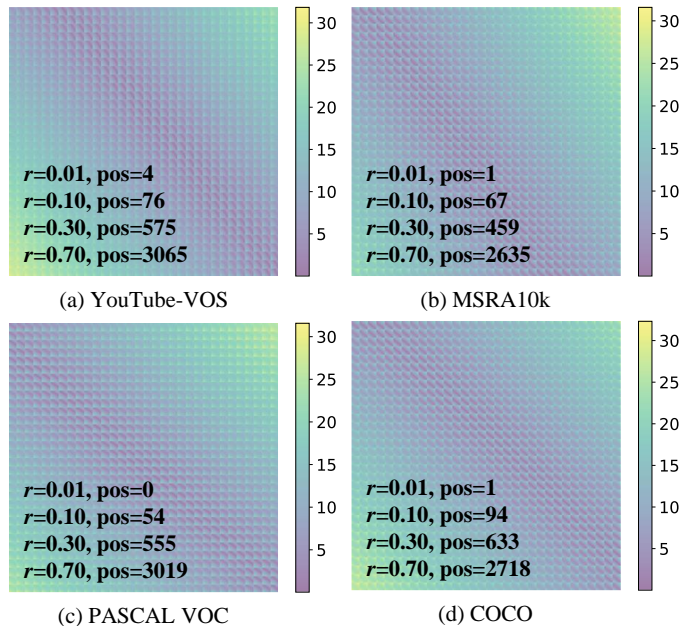


Fig. 8. **Visualization for feature distances** (§4.2) on four crop views from different datasets. ‘pos’ represents the number of positive samples.

VOS (470K). Meanwhile, our method achieves competitive performance on PASCAL VOC (17K) and MSRA10k (10K), which have 28 and 47 times fewer images than YouTube-VOS₁₈. Noteworthy, HVC only requires 0.5h to complete pre-training on PASCAL VOC [79] and has a score of 72.0% $\mathcal{J}\&\mathcal{F}_m$, which is quite close to the state-of-the-art LIIR [4] (72.1% $\mathcal{J}\&\mathcal{F}_m$) trained on YouTube-VOS [26] for 12h. Combining the results of the pre-trained models on each data, we find that setting r to 0.1 always leads to the best results.

Space Projection (Eq. (2)). To elucidate the efficacy of our space projection module, we report the ablation results for different hidden dimensions, as shown in Table 7f. Setting the hidden dimension to 256 yields a highly competitive performance with low computational cost. Employing a larger dimension incurs extra computational overhead during the training process, leading to diminished efficiency with minimal benefit to model performance. The reason is that the space projection module, as the projector head and predictor head for dense features from the backbone,



Fig. 9. **Qualitative results of key modules** (§4.2) for semantic consistency. Given a reference scribbling of the first frame, infer the scribble area in later frames and mark PCK@0.1. Zoomed-in view for best.

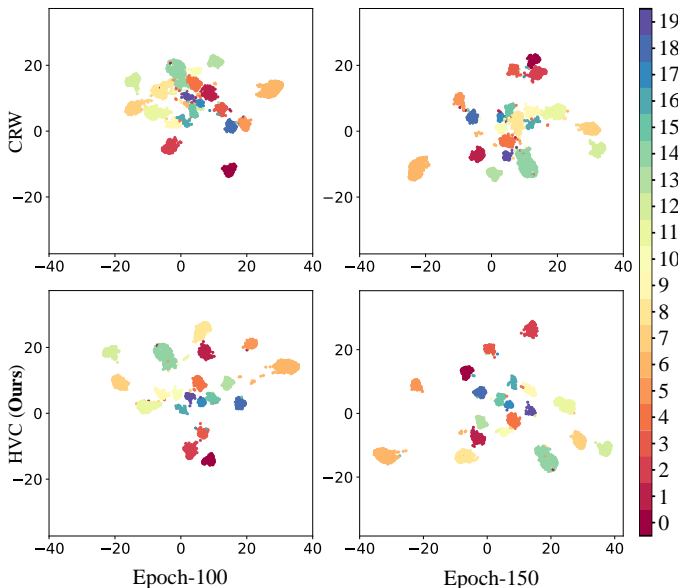


Fig. 10. **Visualization for feature embedding** (§4.3.2) on PASCAL VOC [79] *test-set*. Top: the feature embedding of CRW [1]; Bottom: the feature embedding of our HVC. Zoomed-in view for best.

is limited by the dimension of the original feature channels. Hence, the additional complexity introduced by the larger dimensions might not be effectively applied by the model, especially given the amount and diversity of training data.

Baseline Selection (§3.3) Self-supervised methods designed for image recognition have rich semantic representations. To study the effect of incorporating varied methods (*i.e.*, MoCo [45], PixPro [36], SimSiam [34], and DINO [43]) of semantic self-supervision with the proposed approach, we perform the ablation experiments shown in Table 7g. The initial scores of MoCo and SimSiam are very close. Eventually, MoCo achieves better performance, likely due to the architectural similarities between our HVC and MoCo [45].

4.3 Further Analysis

4.3.1 Efficiency

Achieving optimal video feature representation typically demands extensive video data, leading to prolonged training time and substantial resource consumption. In contrast, our approach utilizes only images to train feature representations while maintaining static-dynamic consistency, striking a balance between performance and complexity. Table 8

TABLE 8

Comparison results (§4.3.1) of computational efficiency. # and Δt denote training iterations and training time, respectively.

Method	Dataset	#	Δt	GPU Memory
ContrastCorr [8]	C + TN	0.4M	1d	44GB
CRW [1]	Kinetics	2M	7d	22GB
DUL [6]	Kinetics	0.3M	2d	12GB
MAST [2]	YT	2M	20h	22GB
LIIR [4]	YT	2M	12h	48GB
DUL [6]	YT	0.1M	16h	12GB
SFC [77]	YT	0.1M	25h	20GB
HVC-YT (ours)	YT	0.1M	7h	16GB
HVC (ours)	C	0.05M	2h	16GB

TABLE 9

Quantitative results for video object segmentation (§4.3.3) on DAVIS₁₇ [25] *test-set*.

Method	Sup.	$\mathcal{J} \& \mathcal{F}_m \uparrow$	$\mathcal{J}_m \uparrow$	$\mathcal{J}_r \uparrow$	$\mathcal{F}_m \uparrow$	$\mathcal{F}_r \uparrow$
CRW [1]	✗	55.9	52.3	-	59.6	-
VFS [3]	✗	57.3	53.1	-	61.6	-
SCC [5]	✗	59.9	55.9	63.9	64.0	72.7
HVC-YT (ours)	✗	61.8	57.3	64.7	66.3	74.9
HVC (ours)	✗	61.7	57.5	65.4	66.0	74.8

presents a comprehensive analysis of the training efficiency of HVC and other methods, considering factors such as training iterations, time, and GPU memory usage. Remarkably, our method achieves state-of-the-art performance using only static image data as training data while requiring little training time (2h) and GPU memory resources (16GB).

4.3.2 Visualization of Feature Tracking and Embedding

In this experiment, we delve deeper into the effectiveness of the learned feature representation by the proposed model on label propagation and image recognition tasks. **1)** As shown in Fig. 9, we replace the first frame annotation with scribbling and subsequently infer the propagation results of this reference mask in the following frames. The learned correspondence by HVC is more detail-oriented, resulting in superior performance compared to its static and dynamic variants. **2)** Fig. 10 depicts low-dimensional embedding visualization of HVC on PASCAL VOC [79]. Our approach has better feature discrimination than CRW [1]. Employing the UMAP [99] training mode, the projection of the categories becomes more accurate as the training proceeds. These findings demonstrate that the learned feature representation is highly effective, even in recognition tasks (non-dense tasks).

4.3.3 Experiments on Additional VOS Datasets

Quantitative Results. We further expand the evaluation of HVC and compare it with state-of-the-art self-supervised methods on more challenging datasets. We present the qualitative results of our method on DAVIS₁₇ [25] *test-set* in Table 9. This dataset consists of 30 video sequences with a higher occlusion frequency compared to DAVIS₁₇ *val-set*. HVC achieves an impressive score of 61.7% $\mathcal{J} \& \mathcal{F}_m$, surpassing existing self-supervised methods. Specifically, our approach shows a 1.8% improvement over SCC [5]. Furthermore, we evaluate HVC on the YouTube-VOS₁₉ version [47], which includes 507 validation videos. The results presented

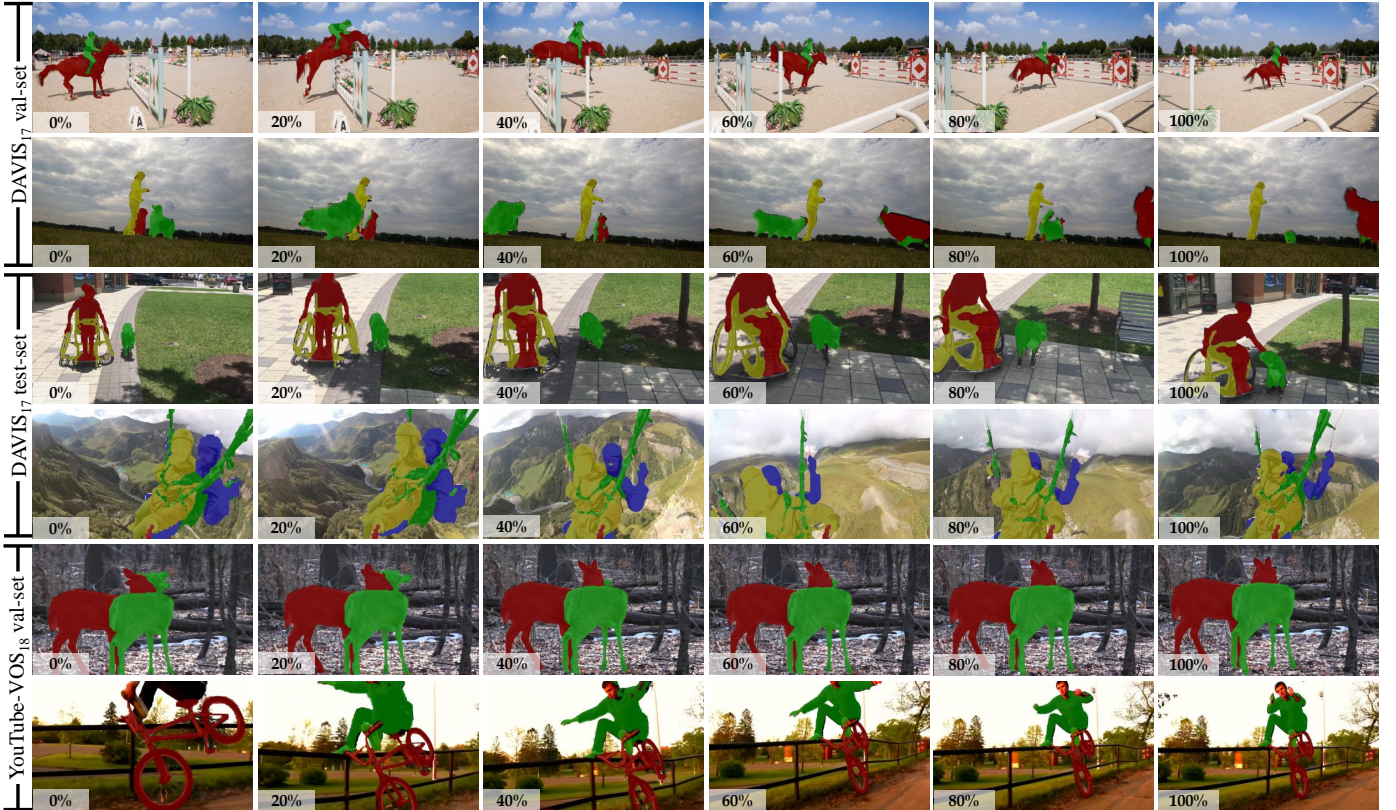


Fig. 11. **Additional qualitative results for video object segmentation** (§4.3.3). The video progress status is shown from 0% to 100% with an interval of 20%. The test video sequences are from the DAVIS₁₇ val-set, DAVIS₁₇ [25] test-set, and YouTube-VOS₁₈ [26] val-set. The feature representation capability of our proposed HVC yields delicate segmentation results in multiple challenging datasets.

TABLE 10
Quantitative results for video object segmentation (§4.3.3) on YouTube-VOS₁₉ [47] val-set.

Method	Sup.	Mean	Seen		Unseen	
			$\mathcal{J}_m \uparrow$	$\mathcal{F}_m \uparrow$	$\mathcal{J}_m \uparrow$	$\mathcal{F}_m \uparrow$
Colorization [21]	✗	39.0	43.3	38.2	36.6	37.5
CorrFlow [9]	✗	47.0	51.2	46.6	44.5	45.9
MAST [2]	✗	64.9	64.3	65.3	61.5	68.4
HVC-YT (ours)	✗	71.3	69.2	70.9	67.8	77.2
HVC (ours)	✗	71.6	69.5	71.2	68.2	77.4

in Table 10, showing that HVC significantly outperforms existing methods in terms of performance.

Qualitative Results. To further showcase the efficacy of our self-supervised approach in video object segmentation, we provide supplementary qualitative results. As illustrated in Fig. 11, we present the qualitative outcomes generated from mask propagation using HVC on three datasets: DAVIS₁₇ [25] val-set, DAVIS₁₇ [25] test-set, and YouTube-VOS₁₈ [26] val-set. The application of learned feature representations, facilitated by our HVC, yields notable performance across a spectrum of complex video sequences.

4.3.4 Pseudo-Dynamic Signals

Our method employs two streamlined convolutional layers (see §3.2.2 for details) to calculate pseudo-dynamic signals, resembling optical flows, amongst cropped image views. This minimalist design circumvents overcomplication of the model while maintaining optimal performance.

TABLE 11
Quantitative results of proposed pseudo-dynamic module (§4.3.4) on DAVIS₁₇ [25] val-set and YouTube-VOS₁₈ [26] val-set. ‘Δ’ means the estimated gap between our HVC and off-the-shelf models.

Off-the-Shelf	Direction	DAVIS ₁₇	YouTube-VOS ₁₈
		EPE ↓	EPE ↓
ΔHVC-RAFT [100]	Forward	6.52	13.18
	Backward	5.71	13.13
ΔHVC-PWC [101]	Forward	5.10	6.88
	Backward	4.49	6.83

Quantitative Analysis. We utilize the off-the-shelf models (e.g., RAFT [100] and PWC [101]) for optical flow estimates on the DAVIS [25] and YouTube-VOS₁₈ [26] validation sets as a ground truth benchmark. We then apply our module $\mathcal{F}_{\text{pseudo}}$ (Eq. (6)) to these datasets to produce dynamic signal estimations. As shown in Table 11, the gap in the End-Point Error (EPE) metric between our self-supervised method and these supervised models is relatively small, signifying that our pseudo-dynamic signal estimations are competitive.

Qualitative Analysis. Following the standardized visualization method proposed in [102], we transform the color space from $2 \times H \times W$ to $3 \times H \times W$. Fig. 12 illustrates the visualization of pseudo-dynamic signals in use on YouTube-VOS [26] and DAVIS [25] datasets. Mirroring the functionality of inter-frame optical flow, our proposed pseudo-dynamic signals between cropped views effectively capture motion cues to maintain dynamic consistency. This assures static-dynamic coherence which in turn enhances

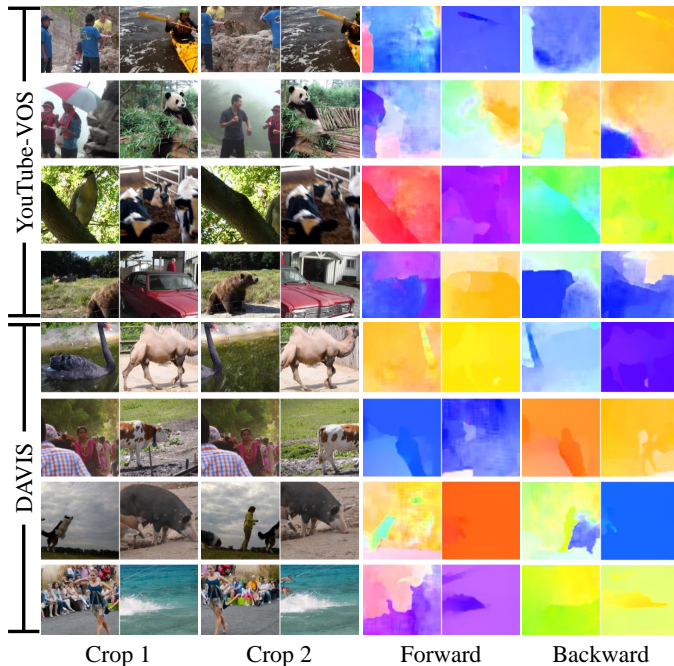


Fig. 12. **Pseudo-dynamic signal visualization** (§4.3.4) on YouTube-VOS [26] (Top) and DAVIS [24] (Bottom). ‘Forward’ and ‘Backward’ indicate the forward and backward pseudo-dynamic signals of ‘Crop1’ and ‘Crop2’ from one image, respectively. Zoomed-in view for best.

the performance of self-supervised feature representation models initially trained on image data.

5 LIMITATION ANALYSIS AND DISCUSSION

Our study presents a hybrid static-dynamic visual correspondence approach that mitigates the influence of uncertain self-supervised signals impeding model convergence. However, it encounters challenges inherent to VOS, such as modeling long-term video sequences and dealing with significant appearance changes caused by occlusion or deformation. Especially, the lack of bespoke pre-training data for intricate scenarios amplifies these challenges.

Long-Term Correspondence. Drawing insights from [73], [84] of leveraging motion chains, we realize an opportunity to refine our approach. Integrating concepts from their iterative knowledge exchange framework can potentially enrich object discovery over vast temporal extents. This can offer a robust solution to a noted limitation of our method: visual correspondences merely between adjacent frames.

Pseudo-Dynamic Generation. Recently, the generation of pseudo-frames from static images has become feasible, aiding video representation learning via readily available diffusion techniques [103]–[106]. Thus, our future research will focus on scalable diffusion techniques in self-supervised VOS, aimed at generating controllable pseudo-frames and enhancing the robustness of VOS in restricted settings.

6 CONCLUSION

In this paper, we presented HVC, an elegant yet highly efficient self-supervised approach for video object segmentation. In contrast to previous approaches that rely on large amounts of training data or complex frame reconstruction

methods, our approach achieved superior performance and efficiency by leveraging an image-based self-supervised representation learning paradigm, such as MoCo [45]. By simulating the dynamic signal presented in video data through image-cropped views, HVC ensured static-dynamic consistency in hybrid visual correspondence learning for VOS. Across multiple benchmark datasets, HVC, trained using only static images, surpassed existing state-of-the-art self-supervised methods that were trained on videos. Moreover, our approach demonstrated the applicability of image-based correspondence learning [36], [43] for video segmentation tasks. We hope the proposed method provides an alternative perspective for self-supervised video object segmentation, opening up new possibilities for utilizing static images in the learning process.

REFERENCES

- [1] A. Jabri, A. Owens, and A. A. Efros, “Space-time correspondence as a contrastive random walk,” in *Proc. Advances Neural Inf. Process. Syst.*, vol. 33, 2020, pp. 19 545–19 560.
- [2] Z. Lai, E. Lu, and W. Xie, “Mast: A memory-augmented self-supervised tracker,” in *Proc. IEEE Conf. Comput. Vis. Pattern Recognit.*, 2020, pp. 6479–6488.
- [3] J. Xu and X. Wang, “Rethinking self-supervised correspondence learning: A video frame-level similarity perspective,” in *Proc. IEEE Int. Conf. Comput. Vis.*, 2021, pp. 10 075–10 085.
- [4] L. Li, T. Zhou, W. Wang, L. Yang, J. Li, and Y. Yang, “Locality-aware inter- and intra-video reconstruction for self-supervised correspondence learning,” in *Proc. IEEE Conf. Comput. Vis. Pattern Recognit.*, 2022, pp. 8719–8730.
- [5] J. Son, “Contrastive learning for space-time correspondence via self-cycle consistency,” in *Proc. IEEE Conf. Comput. Vis. Pattern Recognit.*, 2022, pp. 14 679–14 688.
- [6] N. Araslanov, S. Schaub-Meyer, and S. Roth, “Dense unsupervised learning for video segmentation,” in *Proc. Advances Neural Inf. Process. Syst.*, vol. 34, 2021, pp. 25 308–25 319.
- [7] L. Li, W. Wang, T. Zhou, J. Li, and Y. Yang, “Unified mask embedding and correspondence learning for self-supervised video segmentation,” in *Proc. IEEE Conf. Comput. Vis. Pattern Recognit.*, 2023, pp. 18 706–18 716.
- [8] N. Wang, W. Zhou, and H. Li, “Contrastive transformation for self-supervised correspondence learning,” in *AAAI Conference on Artificial Intelligence*, vol. 35, no. 11, 2021, pp. 10 174–10 182.
- [9] Z. Lai and W. Xie, “Self-supervised learning for video correspondence flow,” in *Proc. British Mach. Vis. Conf.*, 2019.
- [10] R. Li and D. Liu, “Spatial-then-temporal self-supervised learning for video correspondence,” in *Proc. IEEE Conf. Comput. Vis. Pattern Recognit.*, 2023, pp. 2279–2288.
- [11] Y. Yao, T. Chen, G.-S. Xie, C. Zhang, F. Shen, Q. Wu, Z. Tang, and J. Zhang, “Non-salient region object mining for weakly supervised semantic segmentation,” in *Proc. IEEE Conf. Comput. Vis. Pattern Recognit.*, 2021, pp. 2623–2632.
- [12] Z. Zhao, Y. Jin, and P.-A. Heng, “Modelling neighbor relation in joint space-time graph for video correspondence learning,” in *Proc. IEEE Int. Conf. Comput. Vis.*, 2021, pp. 9960–9969.
- [13] R. Li, Y. Wang, L. Wang, H. Lu, X. Wei, and Q. Zhang, “From pixels to semantics: Self-supervised video object segmentation with multi-perspective feature mining,” *IEEE Trans. Image Process.*, vol. 31, pp. 5801–5812, 2022.
- [14] R. Zhang, Z. Jiang, Z. Guo, S. Yan, J. Pan, H. Dong, P. Gao, and H. Li, “Personalize segment anything model with one shot,” *arXiv preprint arXiv:2305.03048*, 2023.
- [15] Z. Yin and J. Shi, “Geonet: Unsupervised learning of dense depth, optical flow and camera pose,” in *Proc. IEEE Conf. Comput. Vis. Pattern Recognit.*, 2018, pp. 1983–1992.
- [16] N. Ye, C. Wang, H. Fan, and S. Liu, “Motion basis learning for unsupervised deep homography estimation with subspace projection,” in *Proc. IEEE Int. Conf. Comput. Vis.*, 2021, pp. 13 117–13 125.
- [17] H. Xu, J. Zhang, J. Cai, H. Rezatofghi, and D. Tao, “Gmflow: Learning optical flow via global matching,” in *Proc. IEEE Conf. Comput. Vis. Pattern Recognit.*, 2022, pp. 8121–8130.

- [18] B. Yan, Y. Jiang, P. Sun, D. Wang, Z. Yuan, P. Luo, and H. Lu, "Towards grand unification of object tracking," in *Proc. Eur. Conf. Comput. Vis.*, 2022, pp. 733–751.
- [19] Y. Cheng, L. Li, Y. Xu, X. Li, Z. Yang, W. Wang, and Y. Yang, "Segment and track anything," *arXiv preprint arXiv:2305.06558*, 2023.
- [20] J. Cao, J. Pang, X. Weng, R. Khirodkar, and K. Kitani, "Observation-centric sort: Rethinking sort for robust multi-object tracking," in *Proc. IEEE Conf. Comput. Vis. Pattern Recognit.*, 2023, pp. 9686–9696.
- [21] C. Vondrick, A. Shrivastava, A. Fathi, S. Guadarrama, and K. Murphy, "Tracking emerges by colorizing videos," in *Proc. Eur. Conf. Comput. Vis.*, 2018, pp. 391–408.
- [22] T. Zhou, F. Porikli, D. J. Crandall, L. Van Gool, and W. Wang, "A survey on deep learning technique for video segmentation," *IEEE Trans. Pattern Anal. Mach. Intell.*, vol. 45, no. 6, pp. 7099–7122, 2023.
- [23] R. Miles, M. K. Yucel, B. Manganelli, and A. Saà-Garriga, "Mobilevos: Real-time video object segmentation contrastive learning meets knowledge distillation," in *Proc. IEEE Conf. Comput. Vis. Pattern Recognit.*, 2023, pp. 10480–10490.
- [24] F. Perazzi, J. Pont-Tuset, B. McWilliams, L. Van Gool, M. Gross, and A. Sorkine-Hornung, "A benchmark dataset and evaluation methodology for video object segmentation," in *Proc. IEEE Conf. Comput. Vis. Pattern Recognit.*, 2016, pp. 724–732.
- [25] J. Pont-Tuset, F. Perazzi, S. Caelles, P. Arbelàez, A. Sorkine-Hornung, and L. Van Gool, "The 2017 davis challenge on video object segmentation," *arXiv preprint arXiv:1704.00675*, 2017.
- [26] N. Xu, L. Yang, Y. Fan, J. Yang, D. Yue, Y. Liang, B. Price, S. Cohen, and T. Huang, "Youtube-vos: Sequence-to-sequence video object segmentation," in *Proc. Eur. Conf. Comput. Vis.*, 2018, pp. 585–601.
- [27] X. Wang, A. Jabri, and A. A. Efros, "Learning correspondence from the cycle-consistency of time," in *Proc. IEEE Conf. Comput. Vis. Pattern Recognit.*, 2019, pp. 2566–2576.
- [28] X. Li, S. Liu, S. De Mello, X. Wang, J. Kautz, and M.-H. Yang, "Joint-task self-supervised learning for temporal correspondence," in *Proc. Advances Neural Inf. Process. Syst.*, vol. 32, 2019, pp. 317–327.
- [29] X. Lu, W. Wang, J. Shen, Y.-W. Tai, D. J. Crandall, and S. C. Hoi, "Learning video object segmentation from unlabeled videos," in *Proc. IEEE Conf. Comput. Vis. Pattern Recognit.*, 2020, pp. 8960–8970.
- [30] Z. Wu, Y. Xiong, S. X. Yu, and D. Lin, "Unsupervised feature learning via non-parametric instance discrimination," in *Proc. IEEE Conf. Comput. Vis. Pattern Recognit.*, 2018, pp. 3733–3742.
- [31] S. Jeon, D. Min, S. Kim, and K. Sohn, "Mining better samples for contrastive learning of temporal correspondence," in *Proc. IEEE Conf. Comput. Vis. Pattern Recognit.*, 2021, pp. 1034–1044.
- [32] T. Chen, S. Kornblith, M. Norouzi, and G. Hinton, "A simple framework for contrastive learning of visual representations," in *Proc. ACM Int. Conf. Mach. Learn.*, 2020, pp. 1597–1607.
- [33] J.-B. Grill, F. Strub, F. Altché, C. Tallec, P. Richemond, E. Buchatskaya, C. Doersch, B. Avila Pires, Z. Guo, M. Gheshlaghi Azar *et al.*, "Bootstrap your own latent—a new approach to self-supervised learning," in *Proc. Advances Neural Inf. Process. Syst.*, vol. 33, 2020, pp. 21271–21284.
- [34] X. Chen and K. He, "Exploring simple siamese representation learning," in *Proc. IEEE Conf. Comput. Vis. Pattern Recognit.*, 2021, pp. 15750–15758.
- [35] W. Van Gansbeke, S. Vandenhende, S. Georgoulis, and L. Van Gool, "Revisiting contrastive methods for unsupervised learning of visual representations," in *Proc. Advances Neural Inf. Process. Syst.*, vol. 34, 2021, pp. 16238–16250.
- [36] Z. Xie, Y. Lin, Z. Zhang, Y. Cao, S. Lin, and H. Hu, "Propagate yourself: Exploring pixel-level consistency for unsupervised visual representation learning," in *Proc. IEEE Conf. Comput. Vis. Pattern Recognit.*, 2021, pp. 16684–16693.
- [37] S. Woo, S. Debnath, R. Hu, X. Chen, Z. Liu, I. S. Kweon, and S. Xie, "Convnext v2: Co-designing and scaling convnets with masked autoencoders," in *Proc. IEEE Conf. Comput. Vis. Pattern Recognit.*, 2023, pp. 16133–16142.
- [38] Y. Fang, W. Wang, B. Xie, Q. Sun, L. Wu, X. Wang, T. Huang, X. Wang, and Y. Cao, "Eva: Exploring the limits of masked visual representation learning at scale," in *Proc. IEEE Conf. Comput. Vis. Pattern Recognit.*, 2023, pp. 19358–19369.
- [39] M. Caron, I. Misra, J. Mairal, P. Goyal, P. Bojanowski, and A. Joulin, "Unsupervised learning of visual features by contrast-
ing cluster assignments," *Proc. Advances Neural Inf. Process. Syst.*, vol. 33, pp. 9912–9924, 2020.
- [40] M. Xu, Z. Zhang, H. Hu, J. Wang, L. Wang, F. Wei, X. Bai, and Z. Liu, "End-to-end semi-supervised object detection with soft teacher," in *Proc. IEEE Conf. Comput. Vis. Pattern Recognit.*, 2021, pp. 3060–3069.
- [41] E. Xie, W. Wang, Z. Yu, A. Anandkumar, J. M. Alvarez, and P. Luo, "Segformer: Simple and efficient design for semantic segmentation with transformers," *Proc. Advances Neural Inf. Process. Syst.*, vol. 34, pp. 12077–12090, 2021.
- [42] W. Wang, E. Xie, X. Li, D.-P. Fan, K. Song, D. Liang, T. Lu, P. Luo, and L. Shao, "Pyramid vision transformer: A versatile backbone for dense prediction without convolutions," in *Proc. IEEE Int. Conf. Comput. Vis.*, 2021, pp. 568–578.
- [43] M. Caron, H. Touvron, I. Misra, H. Jégou, J. Mairal, P. Bojanowski, and A. Joulin, "Emerging properties in self-supervised vision transformers," in *Proc. IEEE Int. Conf. Comput. Vis.*, 2021, pp. 9650–9660.
- [44] T. Stegmüller, T. Lebailly, B. Bozorgtabar, T. Tuytelaars, and J.-P. Thiran, "Croc: Cross-view online clustering for dense visual representation learning," in *Proc. IEEE Conf. Comput. Vis. Pattern Recognit.*, 2023, pp. 7000–7009.
- [45] K. He, H. Fan, Y. Wu, S. Xie, and R. Girshick, "Momentum contrast for unsupervised visual representation learning," in *Proc. IEEE Conf. Comput. Vis. Pattern Recognit.*, 2020, pp. 9729–9738.
- [46] A. Dosovitskiy, L. Beyer, A. Kolesnikov, D. Weissenborn, X. Zhai, T. Unterthiner, M. Dehghani, M. Minderer, G. Heigold, S. Gelly *et al.*, "An image is worth 16x16 words: Transformers for image recognition at scale," in *Proc. Int. Conf. Learn. Representations*, 2021.
- [47] L. Yang, Y. Fan, and N. Xu, "Video instance segmentation," in *Proc. IEEE Int. Conf. Comput. Vis.*, 2019, pp. 5188–5197.
- [48] P. Tokmakov, J. Li, and A. Gaidon, "Breaking the 'object' in video object segmentation," in *Proc. IEEE Conf. Comput. Vis. Pattern Recognit.*, 2023, pp. 22836–22845.
- [49] Q. Zhou, X. Liang, K. Gong, and L. Lin, "Adaptive temporal encoding network for video instance-level human parsing," in *ACM MM*, 2018, pp. 1527–1535.
- [50] H. Jhuang, J. Gall, S. Zuffi, C. Schmid, and M. J. Black, "Towards understanding action recognition," in *Proc. IEEE Int. Conf. Comput. Vis.*, 2013, pp. 3192–3199.
- [51] S. W. Oh, J.-Y. Lee, N. Xu, and S. J. Kim, "Video object segmentation using space-time memory networks," in *Proc. IEEE Int. Conf. Comput. Vis.*, 2019, pp. 9226–9235.
- [52] S. Caelles, K.-K. Maninis, J. Pont-Tuset, L. Leal-Taixé, D. Cremers, and L. Van Gool, "One-shot video object segmentation," in *Proc. IEEE Conf. Comput. Vis. Pattern Recognit.*, 2017, pp. 221–230.
- [53] H. K. Cheng and A. G. Schwing, "Xmem: Long-term video object segmentation with an atkinson-shiffrin memory model," in *Proc. Eur. Conf. Comput. Vis.*, 2022, pp. 640–658.
- [54] Y. Zhang, L. Li, W. Wang, R. Xie, L. Song, and W. Zhang, "Boosting video object segmentation via space-time correspondence learning," in *Proc. IEEE Conf. Comput. Vis. Pattern Recognit.*, 2023, pp. 2246–2256.
- [55] G. Pei, F. Shen, Y. Yao, G.-S. Xie, Z. Tang, and J. Tang, "Hierarchical feature alignment network for unsupervised video object segmentation," in *Proc. Eur. Conf. Comput. Vis.*, 2022, pp. 596–613.
- [56] W. Wang, H. Song, S. Zhao, J. Shen, S. Zhao, S. C. Hoi, and H. Ling, "Learning unsupervised video object segmentation through visual attention," in *Proc. IEEE Conf. Comput. Vis. Pattern Recognit.*, 2019, pp. 3064–3074.
- [57] K. Zhang, Z. Zhao, D. Liu, Q. Liu, and B. Liu, "Deep transport network for unsupervised video object segmentation," in *Proc. IEEE Int. Conf. Comput. Vis.*, 2021, pp. 8781–8790.
- [58] G. Pei, Y. Yao, F. Shen, D. Huang, X. Huang, and H.-T. Shen, "Hierarchical co-attention propagation network for zero-shot video object segmentation," *IEEE Trans. Image Process.*, vol. 32, pp. 2348–2359, 2023.
- [59] G. Pei, F. Shen, Y. Yao, T. Chen, X.-S. Hua, and H.-T. Shen, "Hierarchical graph pattern understanding for zero-shot video object segmentation," *IEEE Trans. Image Process.*, vol. 32, pp. 5909–5920, 2023.
- [60] K. Park, S. Woo, S. W. Oh, I. S. Kweon, and J.-Y. Lee, "Per-clip video object segmentation," in *Proc. IEEE Conf. Comput. Vis. Pattern Recognit.*, 2022, pp. 1352–1361.

- [61] H. Seong, S. W. Oh, J.-Y. Lee, S. Lee, S. Lee, and E. Kim, "Hierarchical memory matching network for video object segmentation," in *Proc. IEEE Int. Conf. Comput. Vis.*, 2021, pp. 12 889–12 898.
- [62] H. Seong, J. Hyun, and E. Kim, "Video object segmentation using kernelized memory network with multiple kernels," *IEEE Trans. Pattern Anal. Mach. Intell.*, vol. 45, no. 2, pp. 2595–2612, 2022.
- [63] H. K. Cheng, Y.-W. Tai, and C.-K. Tang, "Modular interactive video object segmentation: Interaction-to-mask, propagation and difference-aware fusion," in *Proc. IEEE Conf. Comput. Vis. Pattern Recognit.*, 2021, pp. 5559–5568.
- [64] F. Perazzi, A. Khoreva, R. Benenson, B. Schiele, and A. Sorkine-Hornung, "Learning video object segmentation from static images," in *Proc. IEEE Conf. Comput. Vis. Pattern Recognit.*, 2017, pp. 2663–2672.
- [65] X. Xu, J. Wang, X. Li, and Y. Lu, "Reliable propagation-correction modulation for video object segmentation," in *AAAI Conference on Artificial Intelligence*, vol. 36, no. 3, 2022, pp. 2946–2954.
- [66] Z. Yang and Y. Yang, "Decoupling features in hierarchical propagation for video object segmentation," in *Proc. Advances Neural Inf. Process. Syst.*, vol. 35, 2022, pp. 36 324–36 336.
- [67] P. Voigtlaender and B. Leibe, "Online adaptation of convolutional neural networks for video object segmentation," in *Proc. British Mach. Vis. Conf.*, 2017.
- [68] K.-K. Maninis, S. Caelles, Y. Chen, J. Pont-Tuset, L. Leal-Taixé, D. Cremers, and L. Van Gool, "Video object segmentation without temporal information," *IEEE Trans. Pattern Anal. Mach. Intell.*, vol. 41, no. 6, pp. 1515–1530, 2018.
- [69] J. Deng, W. Dong, R. Socher, L.-J. Li, K. Li, and L. Fei-Fei, "Imagenet: A large-scale hierarchical image database," in *Proc. IEEE Conf. Comput. Vis. Pattern Recognit.*, 2009, pp. 248–255.
- [70] Y. Tian, D. Krishnan, and P. Isola, "Contrastive multiview coding," in *Proc. Eur. Conf. Comput. Vis.*, 2020, pp. 776–794.
- [71] A. v. d. Oord, Y. Li, and O. Vinyals, "Representation learning with contrastive predictive coding," *arXiv preprint arXiv:1807.03748*, 2018.
- [72] X. Chen, H. Fan, R. Girshick, and K. He, "Improved baselines with momentum contrastive learning," *arXiv preprint arXiv:2003.04297*, 2020.
- [73] E. Haller, A. M. Florea, and M. Leordeanu, "Iterative knowledge exchange between deep learning and space-time spectral clustering for unsupervised segmentation in videos," *IEEE Trans. Pattern Anal. Mach. Intell.*, vol. 44, no. 11, pp. 7638–7656, 2021.
- [74] A. Radford, J. W. Kim, C. Hallacy, A. Ramesh, G. Goh, S. Agarwal, G. Sastry, A. Askell, P. Mishkin, J. Clark *et al.*, "Learning transferable visual models from natural language supervision," in *Proc. ACM Int. Conf. Mach. Learn.*, 2021, pp. 8748–8763.
- [75] C. Zhou, C. C. Loy, and B. Dai, "Extract free dense labels from clip," in *Proc. Eur. Conf. Comput. Vis.*, 2022, pp. 696–712.
- [76] W. He, S. Jamonak, L. Gou, and L. Ren, "Clip-s4: Language-guided self-supervised semantic segmentation," in *Proc. IEEE Conf. Comput. Vis. Pattern Recognit.*, 2023, pp. 11 207–11 216.
- [77] Y. Hu, R. Wang, K. Zhang, and Y. Gao, "Semantic-aware fine-grained correspondence," in *Proc. Eur. Conf. Comput. Vis.*, 2022, pp. 97–115.
- [78] T.-Y. Lin, M. Maire, S. Belongie, J. Hays, P. Perona, D. Ramanan, P. Dollár, and C. L. Zitnick, "Microsoft coco: Common objects in context," in *Proc. Eur. Conf. Comput. Vis.*, 2014, pp. 740–755.
- [79] M. Everingham, L. Van Gool, C. K. Williams, J. Winn, and A. Zisserman, "The pascal visual object classes (voc) challenge," *Int. J. Comput. Vis.*, vol. 88, pp. 303–338, 2010.
- [80] G. Ponimatkin, N. Samet, Y. Xiao, Y. Du, R. Marlet, and V. Lepetit, "A simple and powerful global optimization for unsupervised video object segmentation," in *Proc. IEEE Winter Conference on Applications of Computer Vision*, 2023, pp. 5892–5903.
- [81] S. Ding, W. Xie, Y. Chen, R. Qian, X. Zhang, H. Xiong, and Q. Tian, "Motion-inductive self-supervised object discovery in videos," *arXiv preprint arXiv:2210.00221*, 2022.
- [82] C. Yang, H. Lamdouar, E. Lu, A. Zisserman, and W. Xie, "Self-supervised video object segmentation by motion grouping," in *Proc. IEEE Int. Conf. Comput. Vis.*, 2021, pp. 7177–7188.
- [83] R. Liu, Z. Wu, S. Yu, and S. Lin, "The emergence of objectness: Learning zero-shot segmentation from videos," in *Proc. Advances Neural Inf. Process. Syst.*, vol. 34, 2021, pp. 13 137–13 152.
- [84] E. Haller, A. M. Florea, and M. Leordeanu, "Spacetime graph optimization for video object segmentation," *arXiv preprint arXiv:1907.03326*, 2019.
- [85] Z. Xie, Y. Lin, Z. Yao, Z. Zhang, Q. Dai, Y. Cao, and H. Hu, "Self-supervised learning with swin transformers," *arXiv preprint arXiv:2105.04553*, 2021.
- [86] N. Wang, Y. Song, C. Ma, W. Zhou, W. Liu, and H. Li, "Unsupervised deep tracking," in *Proc. IEEE Conf. Comput. Vis. Pattern Recognit.*, 2019, pp. 1308–1317.
- [87] S. Liu, N. Ye, C. Wang, J. Zhang, L. Jia, K. Luo, J. Wang, and J. Sun, "Content-aware unsupervised deep homography estimation and its extensions," *IEEE Trans. Pattern Anal. Mach. Intell.*, vol. 45, no. 3, pp. 2849–2863, 2022.
- [88] O. J. Hénaff, S. Koppula, E. Shelhamer, D. Zoran, A. Jaegle, A. Zisserman, J. Carreira, and R. Arandjelović, "Object discovery and representation networks," in *Proc. Eur. Conf. Comput. Vis.*, 2022, pp. 123–143.
- [89] K. He, X. Zhang, S. Ren, and J. Sun, "Deep residual learning for image recognition," in *Proc. IEEE Conf. Comput. Vis. Pattern Recognit.*, 2016, pp. 770–778.
- [90] M. Muller, A. Bibi, S. Giancola, S. Alsubaihi, and B. Ghanem, "Trackingnet: A large-scale dataset and benchmark for object tracking in the wild," in *Proc. Eur. Conf. Comput. Vis.*, 2018, pp. 300–317.
- [91] A. Paszke, S. Gross, F. Massa, A. Lerer, J. Bradbury, G. Chanan, T. Killeen, Z. Lin, N. Gimelshein, L. Antiga *et al.*, "Pytorch: An imperative style, high-performance deep learning library," *Proc. Advances Neural Inf. Process. Syst.*, vol. 32, pp. 8024–8035, 2019.
- [92] D. P. Kingma and J. Ba, "Adam: A method for stochastic optimization," in *Proc. Int. Conf. Learn. Representations*, 2015.
- [93] J. Luiten, P. Voigtlaender, and B. Leibe, "Premvos: Proposal-generation, refinement and merging for video object segmentation," in *Asian Conference on Computer Vision*, 2018, pp. 565–580.
- [94] Q. Wang, L. Zhang, L. Bertinetto, W. Hu, and P. H. Torr, "Fast online object tracking and segmentation: A unifying approach," in *Proc. IEEE Conf. Comput. Vis. Pattern Recognit.*, 2019, pp. 1328–1338.
- [95] A. Athar, J. Luiten, A. Hermans, D. Ramanan, and B. Leibe, "Hodor: High-level object descriptors for object re-segmentation in video learned from static images," in *Proc. IEEE Conf. Comput. Vis. Pattern Recognit.*, 2022, pp. 3022–3031.
- [96] Z. Yang, Y. Wei, and Y. Yang, "Associating objects with transformers for video object segmentation," in *Proc. Advances Neural Inf. Process. Syst.*, vol. 34, 2021, pp. 2491–2502.
- [97] J. Song, L. Wang, L. Van Gool, and O. Hilliges, "Thin-slicing network: A deep structured model for pose estimation in videos," in *Proc. IEEE Conf. Comput. Vis. Pattern Recognit.*, 2017, pp. 4220–4229.
- [98] M.-M. Cheng, N. J. Mitra, X. Huang, P. H. Torr, and S.-M. Hu, "Global contrast based salient region detection," *IEEE Trans. Pattern Anal. Mach. Intell.*, vol. 37, no. 3, pp. 569–582, 2014.
- [99] L. McInnes, J. Healy, and J. Melville, "Umap: Uniform manifold approximation and projection for dimension reduction," *arXiv preprint arXiv:1802.03426*, 2018.
- [100] Z. Teed and J. Deng, "Raft: Recurrent all-pairs field transforms for optical flow," in *Proc. Eur. Conf. Comput. Vis.*, 2020, pp. 402–419.
- [101] D. Sun, X. Yang, M.-Y. Liu, and J. Kautz, "Pwc-net: Cnns for optical flow using pyramid, warping, and cost volume," in *Proc. IEEE Conf. Comput. Vis. Pattern Recognit.*, 2018, pp. 8934–8943.
- [102] S. Baker, D. Scharstein, J. Lewis, S. Roth, M. J. Black, and R. Szeliski, "A database and evaluation methodology for optical flow," *Int. J. Comput. Vis.*, vol. 92, pp. 1–31, 2011.
- [103] R. Rombach, A. Blattmann, D. Lorenz, P. Esser, and B. Ommer, "High-resolution image synthesis with latent diffusion models," in *CVPR*, 2022, pp. 10 684–10 695.
- [104] L. Zhang, A. Rao, and M. Agrawala, "Adding conditional control to text-to-image diffusion models," in *Proc. IEEE Int. Conf. Comput. Vis.*, 2023, pp. 3836–3847.
- [105] S. Tang, F. Zhang, J. Chen, P. Wang, and Y. Furukawa, "Mvd-diffusion: Enabling holistic multi-view image generation with correspondence-aware diffusion," in *Proc. Advances Neural Inf. Process. Syst.*, vol. 36, 2023, pp. 51 202–51 233.
- [106] J. Ren, M. Xu, J.-C. Wu, Z. Liu, T. Xiang, and A. Toisoul, "Move anything with layered scene diffusion," in *Proc. IEEE Conf. Comput. Vis. Pattern Recognit.*, 2024.